

General Disclaimer

One or more of the Following Statements may affect this Document

- This document has been reproduced from the best copy furnished by the organizational source. It is being released in the interest of making available as much information as possible.
- This document may contain data, which exceeds the sheet parameters. It was furnished in this condition by the organizational source and is the best copy available.
- This document may contain tone-on-tone or color graphs, charts and/or pictures, which have been reproduced in black and white.
- This document is paginated as submitted by the original source.
- Portions of this document are not fully legible due to the historical nature of some of the material. However, it is the best reproduction available from the original submission.

(NASA-CR-173878) RESEARCH RELATIVE TO HIGH
ENERGY ASTROPHYSICS Final Report, 1 Feb.
1983 - 31 May 1984 (Smithsonian
Astrophysical Observatory) 55 p
HC A04/AF A01

N84-33315

Unclas
20313

USCIB 03B G3/90

RESEARCH RELATIVE TO HIGH ENERGY ASTROPHYSICS

Grant NAG5-294

FINAL REPORT

For the Period February 1, 1983, Through May 31, 1984



August, 1984

Prepared for

National Aeronautics and Space Administration
Goddard Space Flight Center
Greenbelt, Maryland 20771

Smithsonian Institution
Astrophysical Observatory
Cambridge, Massachusetts 02133

The Smithsonian Astrophysical Observatory
is a Member of the
Harvard-Smithsonian Center for Astrophysics

RESEARCH RELATIVE TO HIGH ENERGY ASTROPHYSICS

Grant NAG5-294

FINAL REPORT

For the Period February 1, 1983, Through May 31, 1984

Principal Investigator Associate Director, High Energy Astrophysics Division
Dr. Paul Gorenstein ✓ Dr. Harvey D. Tananbaum ✓

August, 1984

Prepared for

National Aeronautics and Space Administration
Goddard Space Flight Center
Greenbelt, Maryland 20771

Smithsonian Institution
Astrophysical Observatory
Cambridge, Massachusetts 02138

The Smithsonian Astrophysical Observatory
is a Member of the
Harvard-Smithsonian Center for Astrophysics

TABLE OF CONTENTS

| | | |
|-------|---|----|
| 1.0 | INTRODUCTION..... | 1 |
| 1.1 | Role of High Throughput Imaging And Spectroscopy..... | 1 |
| 1.2 | LAMAR's Capabilities..... | 1 |
| 2.0 | BACKGROUND..... | 3 |
| 2.1 | The Original Investigation..... | 3 |
| 2.2 | Experiment Update And Summary Of Present Status..... | 4 |
| 2.2.1 | Summary Of Recent Accomplishments..... | 4 |
| 3.0 | TECHNICAL DISCUSSIONS..... | 5 |
| 3.1 | Thermal Design Considerations..... | 5 |
| 3.2 | Spectroscopy Mode Of Operation..... | 7 |
| 3.2.1 | Introduction..... | 7 |
| 3.2.2 | Effective Area And Resolving Power..... | 8 |
| 3.2.3 | Simulations Of Measurements..... | 10 |
| 3.3 | Pointing System Requirements And Considerations..... | 15 |
| 3.4 | Mirror Module Performance Analysis..... | 18 |
| 3.4.1 | Introduction..... | 18 |
| 3.4.2 | Construction Of The X-ray Mirror..... | 19 |
| 3.4.3 | Interactive Adjustment Of The Figure..... | 19 |
| 3.4.4 | Performance Of The Mirror Brassboard..... | 22 |
| 3.4.5 | Materials And Machining..... | 24 |
| 3.4.6 | Interactive Tuning..... | 27 |
| 4.0 | CONCLUSIONS..... | 30 |
| | APPENDIX I - LAMAR Thermal Precollimator..... | 32 |

FOREWORD

The work summarized in the following sections represent a continuation of the LAMAR Phase B activity initiated in 1978. Following the submission of an Engineering Requirements Document (ERD) and an Investigator Development Plan (IDP) in 1981, the program scheduled C/D start was postponed because of funding problem. A Phase B continuation effort was funded with primary emphasis on detector electronics, mirror module design, and mechanical and electrical interfaces with the shuttle. In addition to these activities, funding was provided under a Grant to address the following Statement of Work:

- A. Thermal, structural, power, environment and stability research for LAMAR type High Energy astrophysics space detection devices.
- B. Addition of spectroscopic imaging modes of operations using either transmission or reflection gratings.
- C. Pointing system research for this type of instrument to establish limits of permissible operations.
- D. Research associated with detector mirror assemblies and thermal, structural impact on measurements.

This report documents the results achieved in the above task areas, and also provides recommendations for continuing the investigation of mirror fabrication, test, and analysis and for further work in mirror module prototype development.

1.0 INTRODUCTION

1.1 Role Of High Throughput Imaging And Spectroscopy

High throughput imaging is essential for the successful completion of many of the objectives of future programs of X-ray astronomy. Large collecting area and good angular resolution are needed to obtain good positions, to form images of diffuse sources, to avoid the limitations of source confusion and to provide high spectral resolution when used in conjunction with dispersive gratings. The function of the high throughput imaging instrument is to collect a sufficient number of photons from all objects, including point-like sources, diffuse sources, and source complexes, to permit an in depth study of morphology, temporal behavior, and spectrum in a reasonable time without the limitations of shot noise, background, and source confusion. In order to obtain results that are sufficiently quantitative for astrophysical investigations, measurements must of necessity be made at a level of statistical significance that is well beyond that needed to merely establish the existence of sources. The instrument would not be used to conduct studies requiring the highest angular resolution, such as deep surveys, or images of jets from active galactic nuclei. For these reasons the X-ray astronomy community endorses the eventual development of a high throughput imaging facility as a companion to AXAF, the high resolution imaging facility.

1.2 LAMAR's Capabilities

The LAMAR Spacelab Experiment offers a set of capabilities that is unique in the pre-AXAF time period. These are summarized in Table 1-1. The mirrors have a large collecting area that exceeds 10^3 cm^2 below 2 keV and exceeds 200 cm^2 at 6 keV. Their on-axis angular resolution, defined as the diameter of a circle encompassing 50% of the energy, will be about one half of a minute of arc. Its 1 degree field of view makes LAMAR well suited to the study of diffuse sources, such as clusters of galaxies, and source complexes, such as stellar associations. These objects are the focus of our scientific studies. In a later section we describe how a high throughput, moderate to high resolution system ($E/\Delta E \sim 100$) of dispersive spectroscopy could be retro-fitted to the system after its initial flight(s) aboard the Space Shuttle. The spectroscopy system would offer a collecting area for dispersive spectroscopy that is a significant fraction of that available for imaging.

Table 1-1

Characteristics of the LAMAR Experiment

| | |
|--|----------------------|
| Energy Range | 0.1 to 10 keV |
| Field of View | 1 degree diameter |
| Effective Area (On Axis, Mirror + Detector) | |
| 0.28 keV | 1006 cm ² |
| 1.5 keV | 950 cm ² |
| 5.0 keV | 260 cm ² |
| 8.0 keV | 70 cm ² |
| Mirror Vignetting Factor | |
| 10 arcmin offaxis | 0.72 |
| 20 arcmin offaxis | 0.45 |
| On Axis Angular Resolution (Mirror + Detector) | |
| 50% Power Diameter in Arcsec | |
| 0.28 keV | 53 |
| 1.5 keV | 35 |
| 5.0 keV | 32 |
| Off Axis Angular Resolution (Mirror + Detector) | |
| at 1.5 keV, 50% Power Diameter in Arcsec | |
| 10 arcmin off axis | 48 |
| 20 arcmin off axis | 66 |
| Energy Resolution of IPC Detector | |
| E/E FWHM in percent | |
| 0.28 keV | 78 |
| 1.5 keV | 33 |
| 6.0 keV | 19 |
| Sources per Beam at Einstein Deep Survey Sensitivity | |
| of 4×10^{-14} ergs cm ² sec ⁻¹ in 0.3 to 3.5 keV band | |
| less than 0.01 on axis | |
| Sensitivity in 10 ⁴ Seconds | |
| (0.2 to 8 keV, AGN spectrum) | |
| 2×10^{-14} ergs cm ² sec ⁻¹ | |
| Time Resolution of IPC Detector | |
| 60 microseconds | |
| Non X-ray Bkgd of Sum of 8 IPC Detectors | |
| Cts sec ⁻¹ arcmin ⁻² 0.2 to 8 keV | |
| 7×10^{-4} | |
| Intrinsic Position Centroiding Capability | |
| (May be limited by statistics) | |
| 5 arcseconds | |

2.0 BACKGROUND

2.1 The Original Investigation

This investigation was originally proposed in October, 1978, in response to an Announcement of Opportunity for experiments for Spacelab with the title "High Sensitivity Cosmic X-ray Observations with a LAMAR Instrument on Spacelab." The salient features of the investigations we proposed were:

- a) observations based upon high throughput imaging with good angular resolution;
- b) modular approach offering low cost per unit effective area compared to high resolution telescopes;
- c) expandability;
- d) development of technology suitable for larger instrument;
- e) evolutionary development offering growth and improvement of spatial and energy resolution through several Spacelab flights;
- f) availability as a multi-user facility for guest observers after initial flight(s).

The motivation for the Spacelab proposal originated in a paper by Gorenstein (1973). That paper discussed the desirability of developing a high throughput X-ray astronomy facility and proposed a feasible method for the realization of this facility by constructing it as a large area modular array of identical telescopes. The telescopes need not be more precisely co-aligned than what is achievable with ordinary machine tolerances. Thus the problem of developing a high throughput imaging X-ray telescope reduces for the most part to one of developing a module which utilizes its aperture efficiently, has good angular resolution, and is low in cost and easy to manufacture in quantity. Furthermore, that original paper described how the Space Shuttle program could provide an evolutionary path for the development of the high throughput facility over several flights. Re-flights would provide the opportunity to increase the effective area and improve the angular resolution and energy resolution of the LAMAR. Eventually there would be an instrument of proven capability and with sufficient power to merit its repackaging as a free-flyer or for deployment for longer periods of time on a space platform.

The circumstances in which the 1978 proposal was written were as follows:

- 1) HEAO-2 (the Einstein Observatory) had not yet been launched.
- 2) The Spacelab AO suggested that the flight would take place in 1982 or

1983.

- 3) The experiment would be accommodated in a Spacelab pallet and should be designed to interface with it.

The high resolution spectroscopy capability of the Einstein Observatory was rudimentary due to the very low throughput of the dispersive gratings and crystals. Yet Einstein results demonstrated that the region below 2 keV was extremely rich in line features of stellar sources and hinted (with results pertaining to active galactic nuclei) that it was also a very fertile region for the study of extra-galactic objects. These results have underscored the need for high resolution spectroscopy, which is obtainable at present only by dispersive means as opposed to the low or moderate resolution of non-dispersive measurements. We discuss the proposed LAMAR spectroscopy capability in Section 3.2 below.

The technical progress we have made since the proposal was submitted allows us to now offer considerably better performance in the instrumentation than was originally proposed. In addition, a pointing system suitable for the LAMAR experiment is now available. The net result of these changes in circumstances has been to increase the number of opportunities for the LAMAR experiment to make a significant contribution to astrophysics.

2.2 Experiment Update And Summary Of Present Status

2.2.1 Summary Of Recent Accomplishments

In this section we summarize what has been accomplished since the experiment study began. A more detailed description of the instrumentation and engineering studies, including performance parameters for the X-ray mirror and detectors, is given in Section 4. The accomplishments include:

- (1) completion of analytic studies of methods for improving the angular resolution of nested plate (Kirkpatrick-Baez) mirrors (Cohen and Gorenstein 1982) and the development of a new methodology offering low cost and a fast rate of production for the construction of mirror modules with good angular resolution and high throughput;
- (2) construction of a mirror assembly brassboard, with much better angular resolution than originally proposed, and the acquisition of equipment needed for the production of the flight mirrors;
- (3) construction and detailed testing of a second generation imaging proportional counter (IPC) prototype with spatial and resolution performance close to theoretical limits;
- (4) development of readout electronics for the IPC and circuit designs for construction of the flight hardware;

- (5) mechanical layout of the LAMAR experiment compatible with attachment to the Cirrus 1A pointing system;
- (6) study of high throughput dispersive spectroscopy system based upon the addition of an array of reflection gratings to existing mirror assemblies and the development of a ray tracing code for simulation of the overall system;
- (7) writing of several data processing routines that would be incorporated into the software for the ground support equipment and data analysis;
- (8) analysis of Einstein data, which has enabled us to sharpen our focus on several key measurements that take advantage of LAMAR's broad energy coverage, large effective area, and spatial resolution over a 1-degree format. This experience has given us a broader scientific perspective to effectively implement an observing program for LAMAR.

On the basis of what has been accomplished we believe that the performance of LAMAR will be significantly better than that originally proposed.

3.0 TECHNICAL DISCUSSIONS

3.1 Thermal Design Considerations

LAMAR is designed to maintain passive/active thermal control independent of other instruments or facilities except electrical thermal control power. Elements of the thermal control system design are:

- a) Multilayer Insulation (MLI) on all non-aperture surfaces to isolate LAMAR from its environment. 24-layer construction of Dacron scrim alternating with 0.25-mil aluminized Mylar is used. The inner layer is 3-mil Mylar, and the outer layer is Beta cloth.
- b) Thermal isolation at structural mounting points. A conventional double-washer configuration of fiberglass-epoxy with a stainless compression bolt will be used at each interface point.
- c) Thermal radiator surfaces with appropriate thermal control coatings, adjacent to the telescope apertures and facing the viewing direction. These radiators are connected to the low voltage power supplies by heat pipes, and provide passive thermal control of the supplies. Radiator construction is of stiffened aluminum sheet, with an outer covering of silver/Teflon second-surface mirror material attached with low-outgassing adhesive. Heat pipes are connected to the radiators by machined saddles.
- d) An insulating thermal precollimator covering each telescope aperture. The term precollimator refers to an assembly of parallel cells of roughly rectangular cross-section, analogous (though not identical) to honeycomb core material. Its purpose is to reduce thermal radiation through the

assembly by restricting radiative viewfactors, but allowing collimated X-rays to pass. The material may be a thermal insulator, as in this case, or thermally-conductive, as described in the next section. A four-cell "shadow box" element is planned for each telescope, with each cell corresponding to one quadrant of the mirror assembly. The material will be a lightweight composite to achieve maximum stiffness while minimizing thermal conductance.

- e) A conductive precollimator between the mirrors and insulating precollimator of each telescope. This precollimator isolates the mirror assembly from the space environment. It is the primary thermal control surface of LAMAR, contains heaters for active thermal control, and is also the sink for the heat pipes connected to the detectors. The conductive precollimator is comprised of rectangular thin-walled aluminum tubes bonded together into a unit assembly inside a rectangular frame. The tube sizes are selected and aluminum sheet spacers added so that the tube walls coincide axially with the mirror plates for minimum vignetting of the aperture.
- f) An active thermal control system for each aperture or group of apertures, consisting of heaters on the conductive precollimator, and a mechanical or electronic thermostat. The controllers are commercially-available military-style electronics in hermetically-sealed packages.
- g) Heat pipes parallel to the axis of the telescopes to transmit heat dissipated in detectors and electronics to the conductive precollimators and to the radiators. Axial-groove, ammonia-filled heat pipes are used; this configuration is well-proven and represents very conservative design. Required capacity is approximately 250 watt-meters, divided among several heat pipes, each operating well below maximum capability for redundancy and assurance of proper priming.
- h) Thermal control coatings on external surfaces that are not easily insulated. A second-surface metallized tape material having low emittance and absorptance/emittance ratio less than one is used. This minimizes heat leak but ensures that no overheating will occur in sun.
- i) Retroreflective surfaces surrounding the outer portion of the apertures to reject incident solar radiation. Use of these surfaces is discussed in a later section.
- j) If permitted by the interface with the pointer, a sheet of flexible material extending to the instrument at approximately sill level, isolating the cavity from the external space environment. This will ensure that externally-imposed thermal loads on all detector assemblies are essentially equivalent.

The present thermal control design concept for LAMAR uses the telescope aperture and the adjacent radiators as the primary thermal control surfaces. Axial heat pipes transport detector and electronics dissipation forward to the conductive precollimator covering the mirror apertures, from which it is radiated to space through the insulating precollimator. Other heat pipes connect low-voltage power supplies to the radiators. An approximate heat balance for the hot case

is achieved by design of the insulating precollimator to control its effective emittance, and active control is exercised at the conductive precollimator for colder cases. The integrating structure holding the telescopes does not participate in thermal control to first order, except to provide the operating environment for the electronics. Ideally the integrating structure would be adiabatic, and is covered with multilayer insulation to approximate this condition. In the general case, however, this large external area represents a positive or negative heat leak, depending on environmental inputs to the surfaces, and the leak will increase the dynamic range of active control required.

A major constraint on precollimator design is that the aperture should radiate full experiment power at 60 degrees to the sun (incident energy about 65 watts/ft²). This constraint implies that the precollimator must reject enough of the solar load at 60° incidence to permit full experiment power to be radiated, so that thermal control may be maintained. Using either diffuse or specular surface coatings will cause at least half the incident load to be scattered or reflected into the precollimator; the aperture cannot radiate this much power plus experiment power at the desired operating temperature. Most of the incident load must therefore be rejected to space without being absorbed, which will require using a surface with retroreflective properties for the protective cover. The baselined configuration has a sawtooth cross-section with specular surfaces. This type of surface will fulfill the design constraint under most pointing conditions. The performance goal is to reject 80% or more of the solar load incident on the aperture. Because of the criticality of the thermal precollimator to LAMAR design, a proof-of-concept model was developed to permit empirical validation of thermal performance. A brief description of this precollimator model, test conditions and results of the thermal test are provided in Appendix 1. The conclusions reached as a result of this test are:

- a) the precollimator is effective in reducing heat flow from a telescope aperture, radiating as a black body, and
- b) performance of a LAMAR precollimator can be predicted with sufficient accuracy by conventional analytical modeling methods.

3.2 Spectroscopy Mode Of Operation

3.2.1 Introduction

LAMAR is designed to accommodate a set of reflection gratings as a simple retrofit. A space of 30 cm in front of the mirrors along the optic axis is left vacant for the gratings. We propose that the gratings be fully incorporated into the instrument for the third flight. A pilot test of the system could be carried out during the second flight, where we propose to add a set of gratings to only one module. The throughput of even one module is so large (about twenty times larger than the OGS of the Einstein Observatory) that there will be ample opportunity to perform measurements that are meaningful with only 20% of the observing time of the mission devoted to dispersive spectroscopy.

The dispersive elements are blazed reflection gratings which function in the conical diffraction mode. They have the same characteristics as the grating described by Cash and Kohnert (1982). The line density is 6000/mm and the blaze angle is 21 degrees. A total of about 400 identical elements would be used to completely fill the apertures of eight LAMAR modules. Their dimensions are 8" x 12" x .02". While the number of grating plates is large, their fabrication is amenable to mass production by a standard replication process. A single master is ruled and is used to make several sub-masters, which are then used to make the flight units. From the standpoint of replication one is essentially making copies of a flat plate—a straight forward process in the optics industry. The alignment of the plates within a modular box is very simple. They are parallel and equally spaced. Standard machine tolerances will suffice for their alignment. The integration of a grating module box to a mirror module is equally straight forward. The apertures of the two match and, ordinary machine tolerances provide sufficient accuracy. A small segment of the grating module will be specularly reflecting. This will cause a point image of the source to appear in the field of view of the detector, off the dispersed spectrum, for the purpose of monitoring the continuum.

3.2.2 Effective Area And Resolving Power

A ray tracing code has been developed for studying the performance of the dispersive spectroscopy system. It is a Monte Carlo program which takes into account all instrument efficiencies and resolution factors, including those of the mirror and detector. In addition to placing gratings in front of the mirror, we would also make two minor modifications to the detector. One is that the window is replaced with 0.5 μ material for improved transmission at 0.5 keV. The University of Wisconsin group has successfully made 0.5 μ windows for proportional counters of much larger area than the 6 cm diameter of our IPCs. They have been used on rocket flights and are scheduled for their DXS Spacelab experiment. Even thinner windows have been made (Huizenga et al. 1981). The other is that the pressure of the gas mixture (and voltage) of the IPC will be changed in a manner that results in a smaller primary electron cloud and in improved spatial resolution in the dimension along the direction of dispersion. This occurs at the expense of some loss of spatial resolution in the other dimension because of quantization on anode wires, but that is of little consequence when the gratings are in place.

Figure 3-1 shows two spot diagrams showing the focal plane image for X-rays at several wavelengths. The upper panel is the first order and includes wavelengths from 16 to 27.4 \AA . The lower panel shows the second order images in the range 8.3 to 17.6 \AA . The locus of wavelengths traces out a segment of an ellipse. Dispersion is nearly linear along the y dimension of the detector. The principal wavelength, in this case 24 \AA , occurs at the focal plane center. First and second order wavelengths will fall at the same position. This is not expected to be a problem in practice because a spectrum will rarely have several lines or features that are exact multiples of each other. Any possible ambiguity in the wavelength of a line would be removed by the pulse height resolution of the IPC. This is good enough not only to distinguish between, for example, lines at 12 and 24 \AA on the basis of their pulse height peaks but also

ORIGINAL QUALITY
OF POOR QUALITY

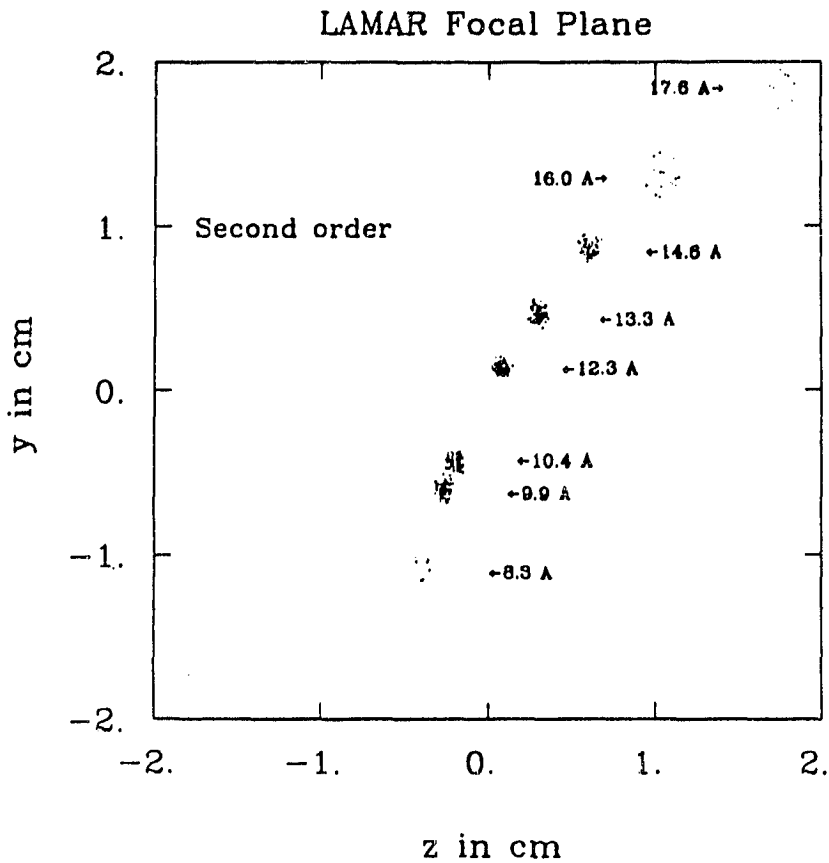
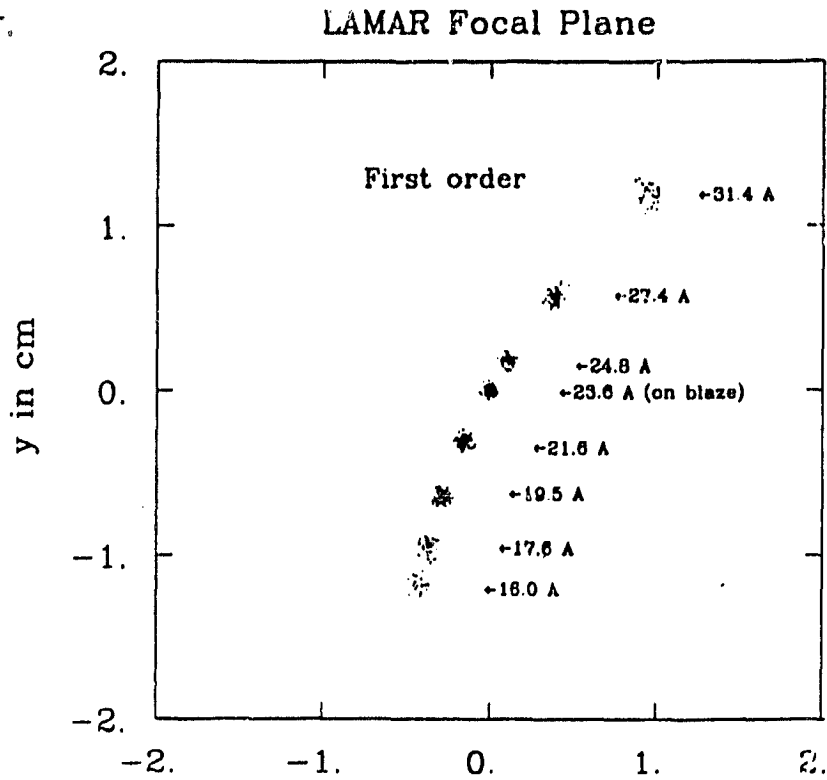


Figure 3-1 Focal plane spot diagrams of various wavelengths when conical diffraction gratings are placed in front of LAMAR mirror. First and second orders are shown.

to resolve them in the rare circumstance that both occur in the same source.

Figure 3-2 shows the effective area and resolving power as a function of wavelength for first and second order. The resolving power is defined as the wavelength interval corresponding to the spatial element containing 50% of the flux from a line divided by the distance between differences of one Å unit in wavelength. The resolving power peaks at about 140 in the center of the detector. The fall off is due partly to the off axis behavior of the mirror and partly to the nature of conical diffraction. However, it is expected to be substantially better than the resolving power of 25 to 50 of the OGS of the Einstein Observatory over a wide range of wavelengths.

The effective area for first and second order reflections is also shown in Figure 3-2. The ray tracing program actually gave twice as much area as that shown, but we have included the experimentally measured values of efficiency by Cash and Kohnert in our simulation of the two orders. We have not included the third order because there is insufficient laboratory data to substantiate the ray tracing results. By comparison, the OGS of Einstein had only about 1 cm² of effective area.

3.2.3 Simulations Of Measurements

To put dispersive spectroscopy with LAMAR within a physical context, we simulated several measurements. Figure 3-3 is a 3×10^6 K thermal spectrum (Raymond-Smith model with cosmic abundances). The upper panel is the input spectrum and the lower panel displays the output of the instrument, including statistical fluctuations. A total of about 3200 photons are detected. This would be obtained in an observing time of 5000 seconds for a number of stellar objects. Figure 3-4 is a similar result for a 3×10^7 K plasma where we plot the second order spectrum. Approximately 2000 counts appear in this spectrum. In both of these figures comparison of the upper and lower panels indicates that we detect most of the features of the input spectra. Figure 3-5 is a simulated observation of a nearby quasar or Seyfert galaxy. In the model we assume that 85% of the photons are due to a power law component with a spectral index in photon number of -1.7. The remainder is a 3×10^6 K thermal component with a cosmic abundance of unity. The thermal component would be associated with an accretion disk or clouds of hot gas around the nucleus. The observing time is 10^4 seconds. Lines are resolved despite the strong contribution from the power law continuum.

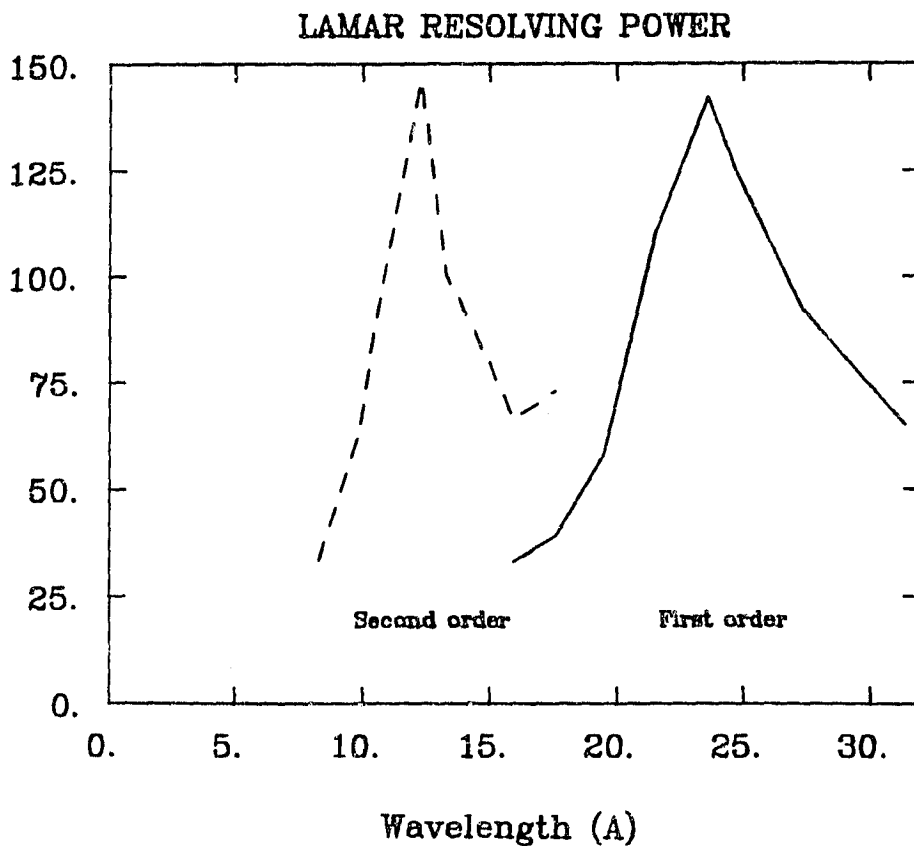
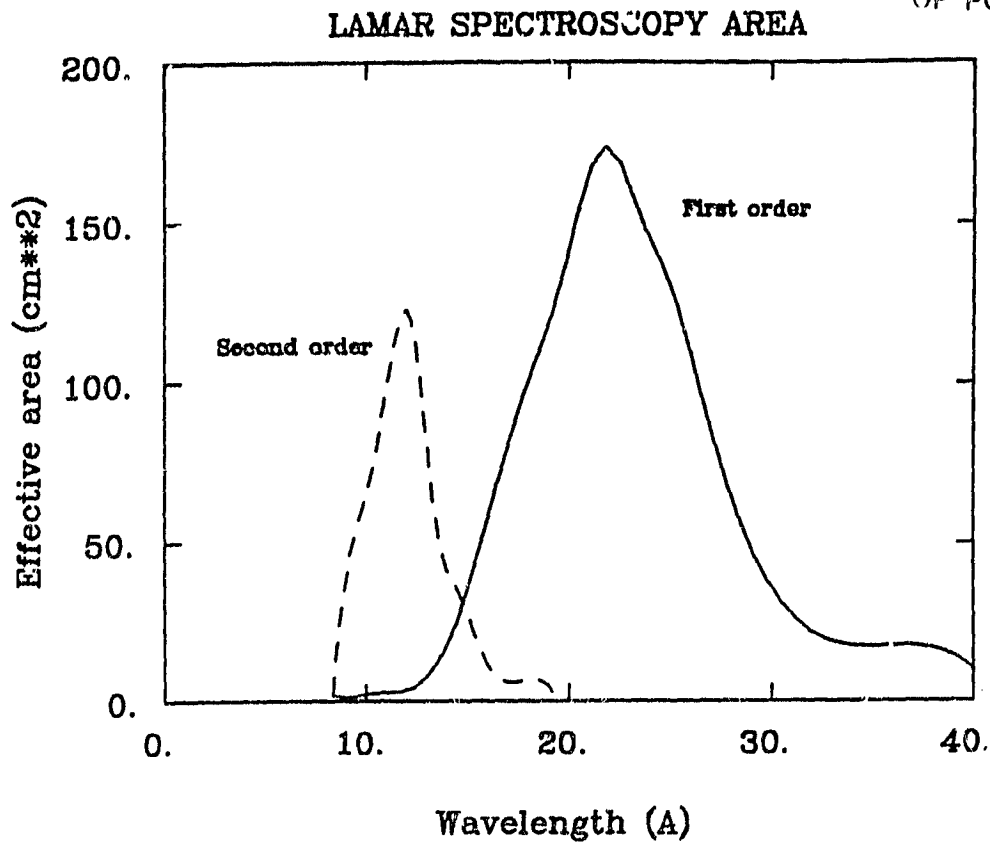
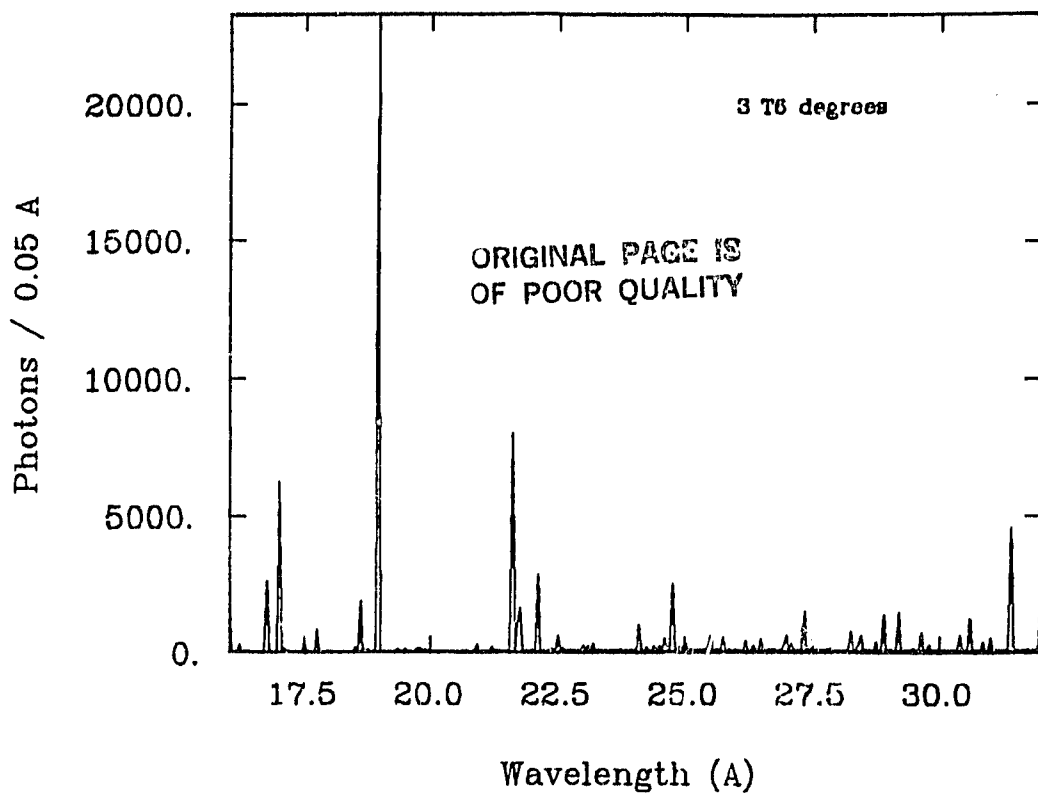


Figure 3-2 Effective area and resolving power of dispersive spectroscopy system for LAMAR as determined from a ray tracing code. Effective area calculation includes laboratory measurements of Cash and Kohnert, 1982. The principal wavelength is 24 Å.

Raymond-Smith Input Spectrum



Raymond-Smith Output Spectrum

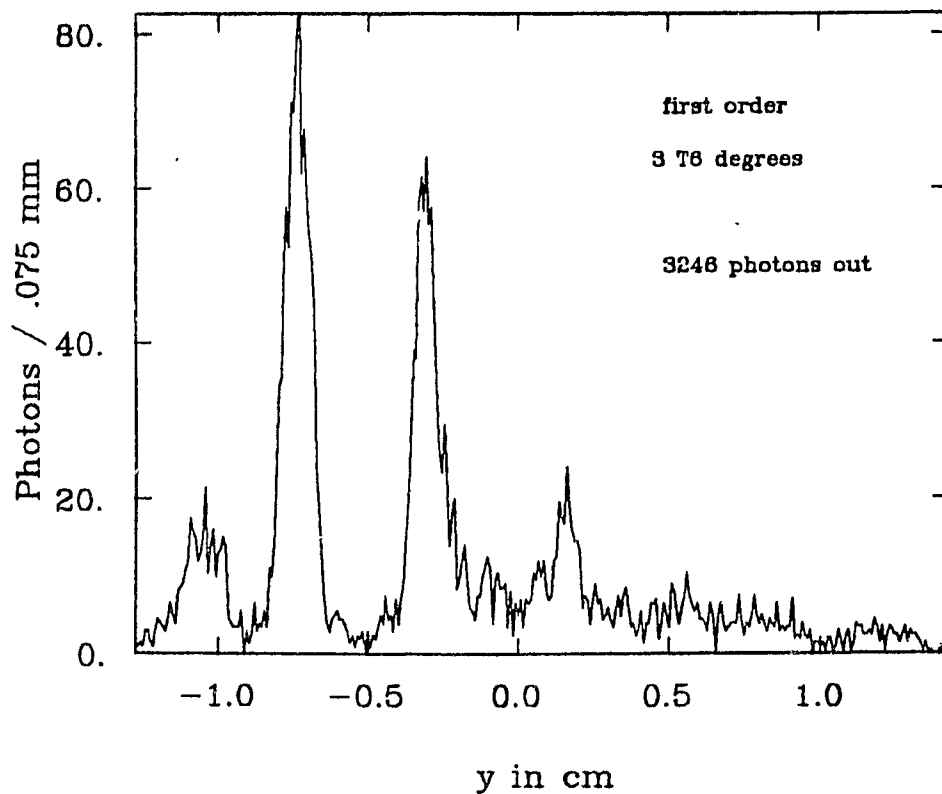
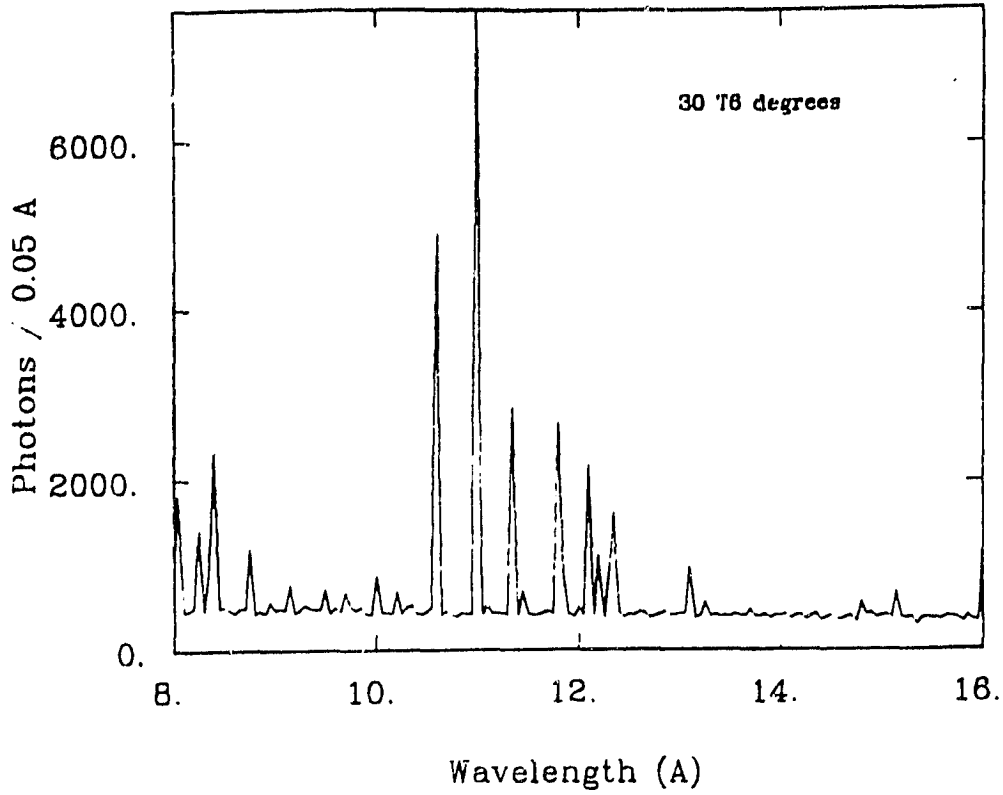


Figure 3-3 Ray tracing simulation of a 3×10^6 h α spectral spectrum as observed in first order. The detected spectrum contains some 3200 counts. Statistical fluctuations are included.

Raymond-Smith Input Spectrum

ORIGINAL PAGE IS
OF POOR QUALITY



Raymond-Smith Output Spectrum

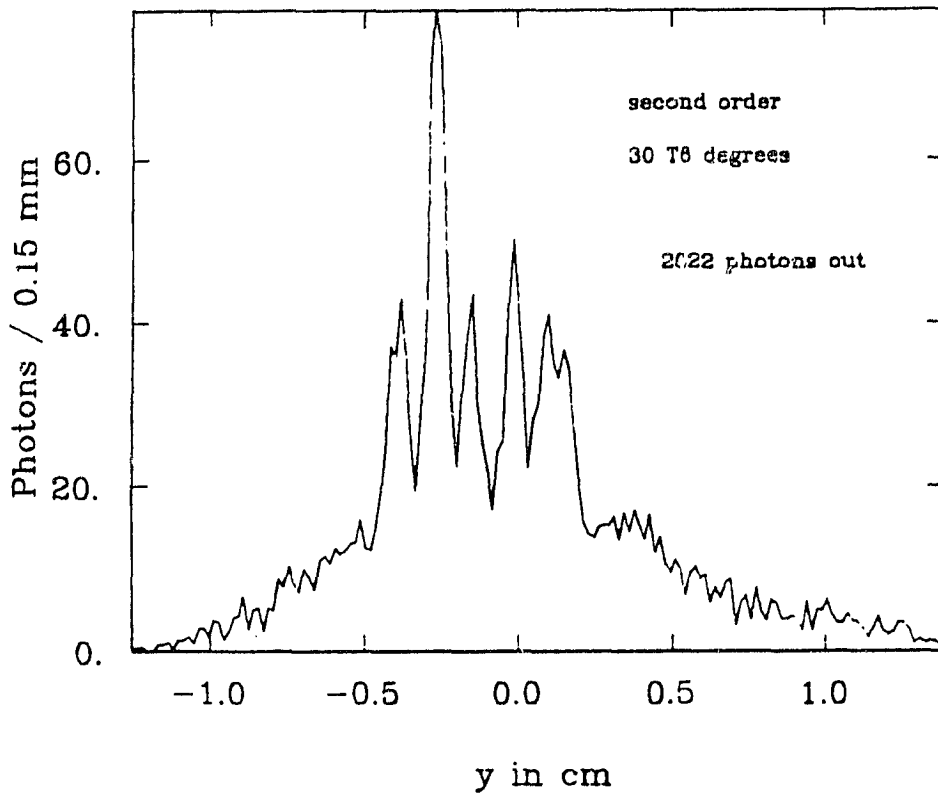
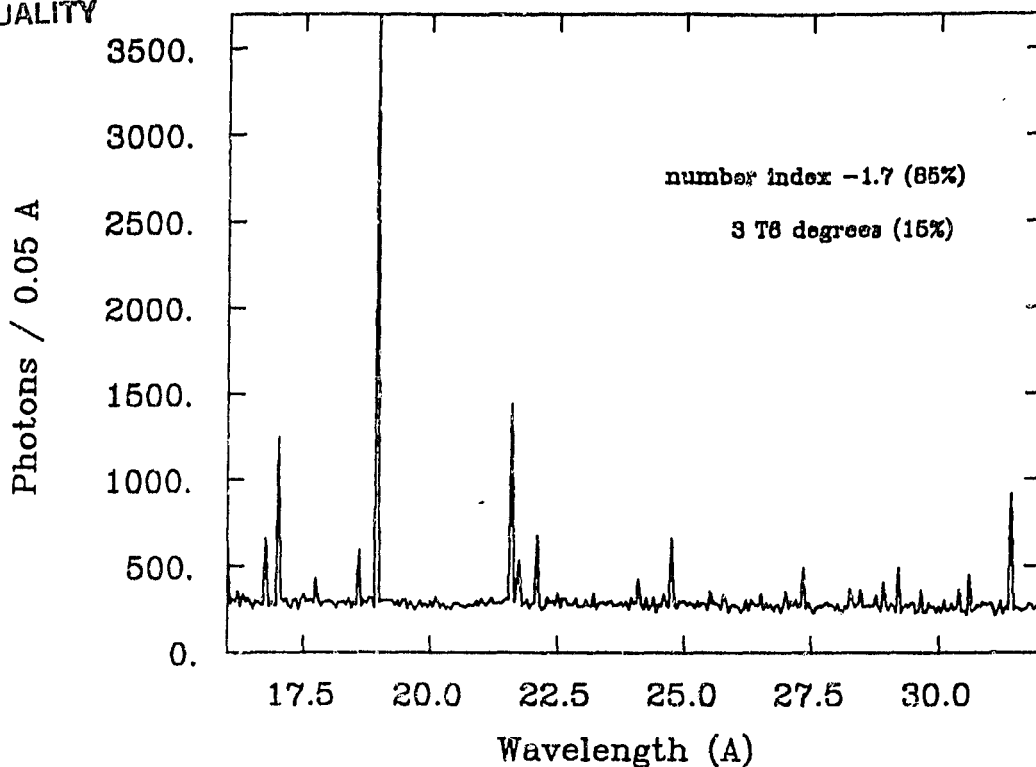


Figure 3-4 Same as Figure A-3 but temperature of thermal plasma is now 3×10^7 K.

Power Law + Thermal Input Spectrum



Power Law + Thermal Output Spectrum

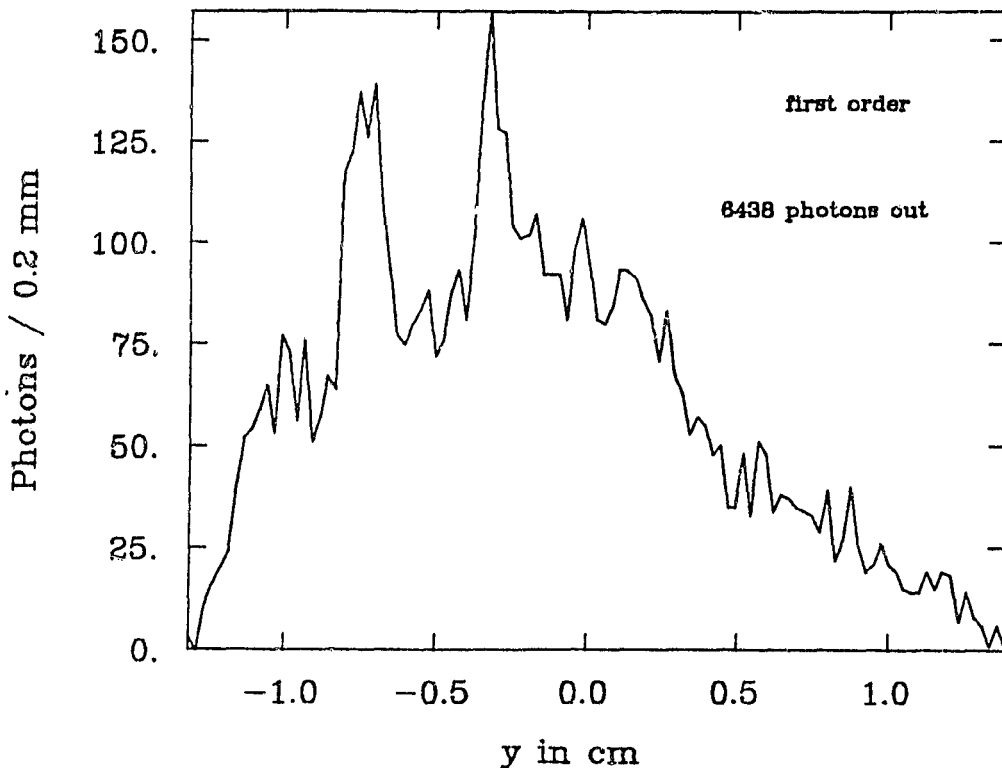


Figure 3-5 Simulated observation of a quasar assumed to have a spectrum consisting of a nonthermal (number spectrum -1.7) and a thermal component (3 million K). 85% of the photons are attributed to the nonthermal spectrum, the remainder to the thermal spectrum. The simulated counts correspond to a 6000 second observation of a 1 cnt/sec Einstein IPC source; statistical fluctuations are included.

3.3 Pointing System Requirements And Considerations

A NASA supported study of the LAMAR experiment began in 1979. Since that time an important change has occurred in how LAMAR would be integrated into the Space Shuttle. According to the concept which prevailed at the time the proposal was written, it would be mounted into a pallet. Recently, a pointing system has

become available which can accommodate LAMAR. This change is very beneficial from our standpoint. The time on target is now more certain for planning an observing program. There is more latitude in target selection so that the sources which are optimum from the standpoint of our objectives have a greater probability of being accessible.

The change from the pallet to the pointing system has resulted in a modification to the dimensions of the experiment and a redistribution of our effective area across the band pass. On the whole, we regard the change as a significant improvement. To fit within the boundaries of the pointing system the gross aperture cannot be as large as before. Consequently, the number of modules must be reduced from the original 16 to 8, and each module is somewhat smaller in gross area. However, the focal length can be longer. Longer focal length provides benefits that more than offset this reduction. It has resulted in more efficient utilization of the aperture, including significantly larger effective area at higher energies. There is improved angular resolution at all energies because the spatial resolution of the detector is a less important factor. Compared to the configuration of the original proposal, the current mirrors have about one-half of the effective area below 0.5 keV (1450 as compared to 2900 cm²), about the same at 2 keV (1100 cm²), and much more above 5 keV. Considering the increase in observing efficiency that results from the use of the pointing system, LAMAR's collecting power is essentially undiminished if not actually increased. Moreover, with the large increase in effective area at high energies, there is a significant improvement in the ability to measure temperature which is required by our experiment objectives.

The instrument to pointer attachment points will be located on the flanges of the metering structure. This location minimizes induced forces from vibration or thermal changes.

The LAMAR instrument will be integrated into the CIRRIS pointer with all components previously mounted and aligned at SAO except for those peripheral components that are outside of the "I" envelope below the instrument center of gravity. These components will be mounted to the metering structure after the LAMAR instrument is integrated with the pointer.

The total weight of the LAMAR instrument is ~895 kg (1969 lb.), which is significantly less than the CIRRIS pointer capability. Because the center of mass of the instrument is within 5 cm of half the instrument length, the inertia about the instrument mounting area will be well within the CIRRIS pointer capability. Adequate clearance is available between the LAMAR instrument and

LAMAR ON CIRRIS POINTER

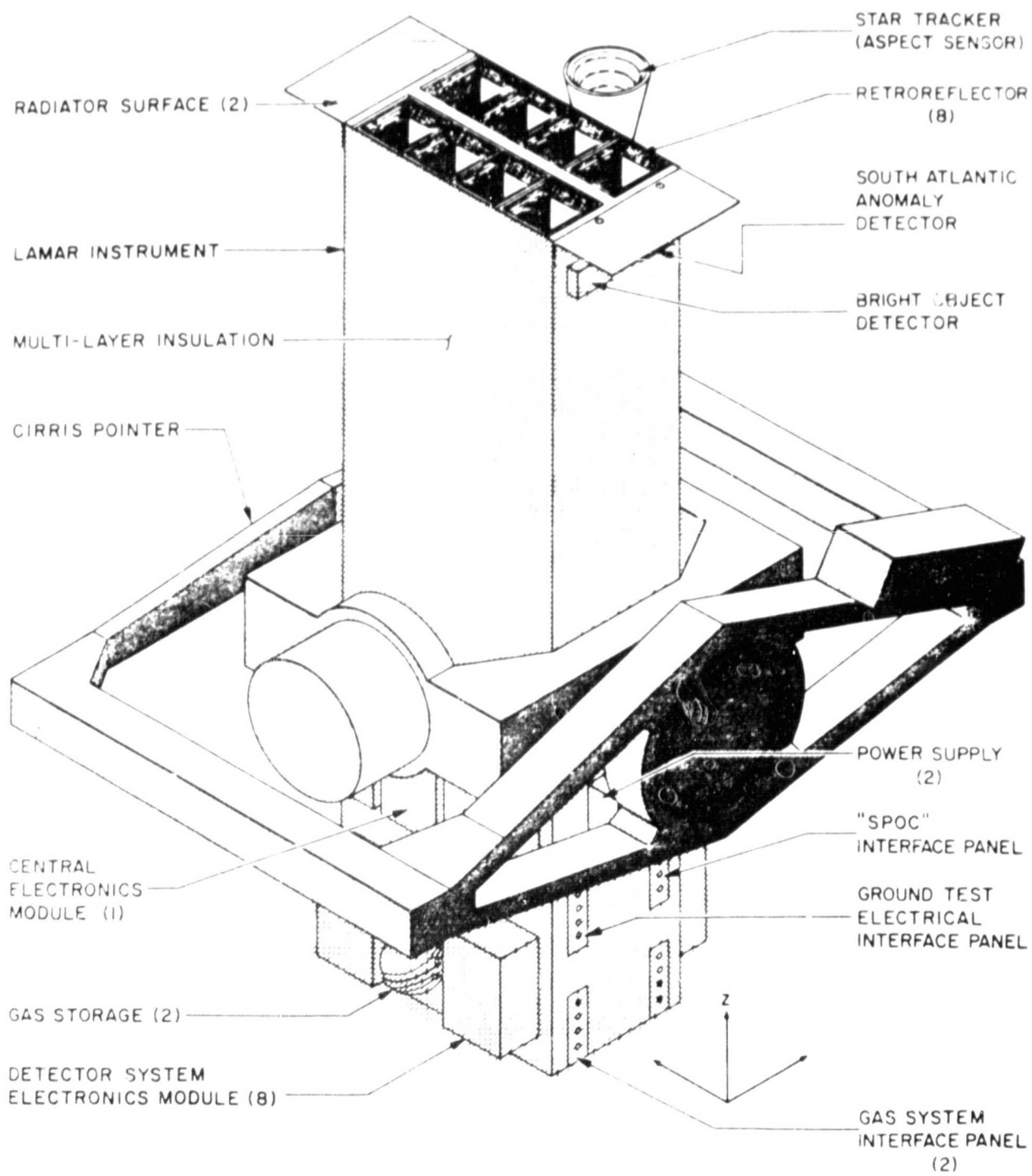
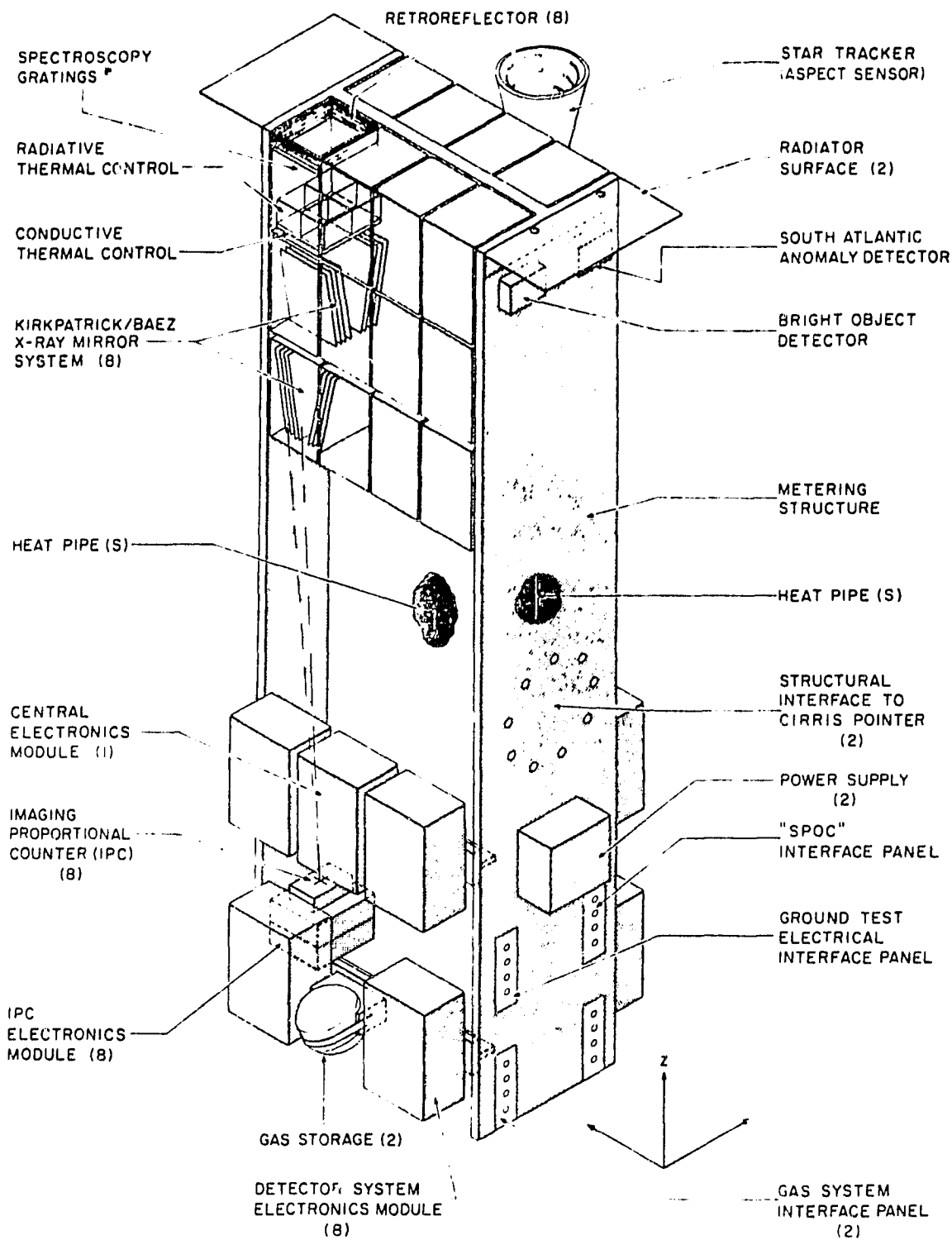


FIGURE 3-6

LAMAR EXPERIMENT

ORIGINALLY DESIGNED
OF POOR QUALITY



*to be added for future flights

FIGURE 3-7

the orbiter outer dynamic envelope.

3.4 Mirror Module Performance Analysis

3.4.1 Introduction

The LAMAR experiment contains eight mirror modules, each with a frontal area of 9 x 12 inches. This is the maximum number with these dimensions that can be accommodated within the boundaries of the CIRRUS 1A pointing system. With the focal length fixed at essentially the largest dimension that will fit within the dynamic envelope of the Shuttle bay, the optimum trade-off between the number of modules and their size is determined by how one wishes to distribute the effective area across the 0.1 to 10 keV band. Our objectives require a rather broad bandwidth with sufficient collecting area above 5 keV to permit spatially resolved temperature measurements of kT in the range 2-10 keV for diffuse sources and for individual members of source complexes as well as very large area below 2 keV for eventual dispersive spectroscopy measurements.

The mirror modules are of the "Kirkpatrick-Baez" type. They consist of two successive orthogonal arrays of nested plates which are curved slightly in one dimension to conform to co-axial parabolas.

The advantages of this type of mirror module are as follows:

1. In comparison to a high resolution mirror such as AXAF, the cost is very low, the aperture utilization is more efficient, and the weight is about one fifth as much for the same effective area while the angular resolution is sufficiently good for satisfying many scientific objectives such as those of this investigation.
2. The reflecting surfaces are flats and can be an inexpensive commercial material in which no polishing is required to produce excellent X-ray properties. The material in our system is 70 mil thick float glass overcoated with gold or nickel, which (as shown in our original proposal) has a reflection efficiency that is unsurpassed and has very low scattering.
3. The process of figure formation can be addressed by an objective method that utilizes sensor mediated "semi-intelligent" computer assistance rather than machining requiring tight tolerances. The procedure is straight forward, very accurate, and is capable of a fast production rate.

The angular resolution of the Kirkpatrick-Baez mirror is very good when the reflecting plates conform to parabolas. We have developed an objective procedure for achieving the desired parabolic shape. This procedure has two key components. One is a technique for pre-curving a mirror plate uniformly to

approximately the correct shape with little distortion. The other is interactive tuning of the figure of a mirror plate in the presence of a large area parallel light beam. With pre-curving, tuning is then only a process of differential correction. A microcomputer is used in the tuning process to provide a digital indication of how much the image position deviates from the desired value. Our experience with the LAMAR mirror brassboard indicates that the accuracy of the method is very high and that the limiting factor in the quality of the image is the flatness of the original glass material.

We believe that the procedure we use is not merely an interim technology for a comparatively modest LAMAR experiment. It is capable of programing a large number of modules and is applicable without modification and without much increase in cost to modules of larger size. There is likely to be a desire to make larger modules in the future when longer focal lengths are available on a free-flyer or Space Station for a high throughput facility. One merely applies the same methods to larger sheets of material. In fact, the technique is even more effective when scaled up to larger sizes. As neither the thickness of the sheets nor their minimum separation need increase larger, longer focal length mirrors are likely to be even more efficient with respect to aperture utilization and low weight per unit effective area.

3.4.2 Construction Of The X-ray Mirror

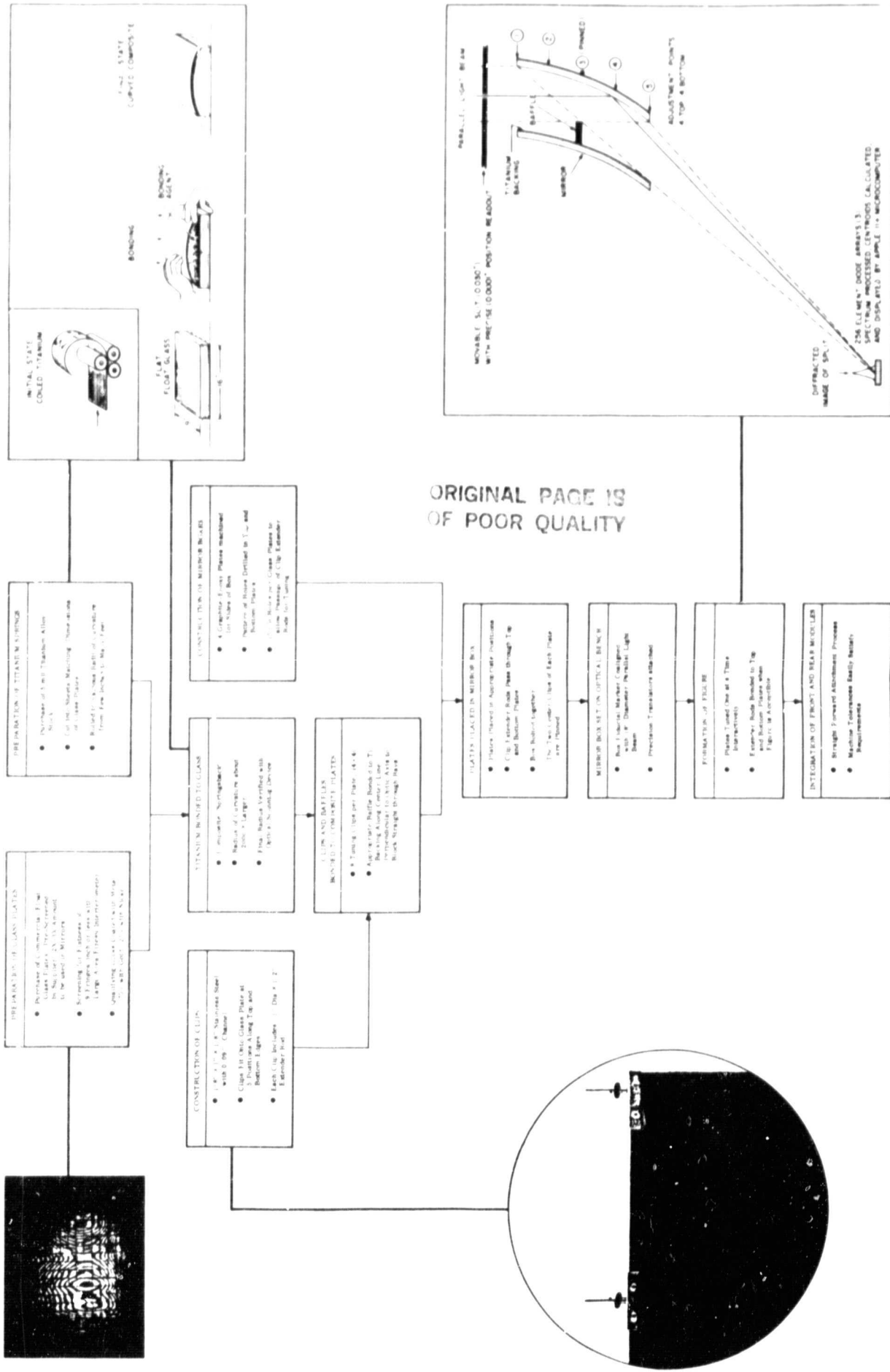
Figure 3-8 is a flow diagram illustrating the sequence of events which take place in the construction of a LAMAR mirror module. All of the materials involved are commercially available from a wide variety of sources. None of the machining operations involve more than ordinary tolerances.

3.4.3 Interactive Adjustment Of The Figure

The figure of each plate is optimized by interactive adjustment or tuning in visible light. Small forces are applied to the extender rods at four points along two edges of the plate. A fifth point in the middle is pinned. With the curvature of the glass titanium-composite approximately equal to the mean radius of the ideal parabola, the effect of the tuning process is merely to make small, differential changes from the initial condition.

The tuning procedure is illustrated in Figure 3-9. A parallel light beam about 18 inches in diameter is established at one end of an optical bench with the use of a He-Ne laser, beam expander, and a large parabolic mirror. The assembly of mirror plates is mounted several feet along the optical bench on a sturdy holding fixture. Plates are tuned one at a time in the following way. A motor driven slit limits the visible light beam to a region amounting to about one-sixth of the area of the plate. (The slit width is varied from plate to plate to maintain that fraction.) A readout stage displays the slit's absolute

SEQUENCE OF EVENTS IN CONSTRUCTION OF LAMAR MIRRORS



ORIGINAL PAGE IS OF POOR QUALITY

FIGURE 3-8

PROCEDURE FOR TUNING MIRROR PLATES

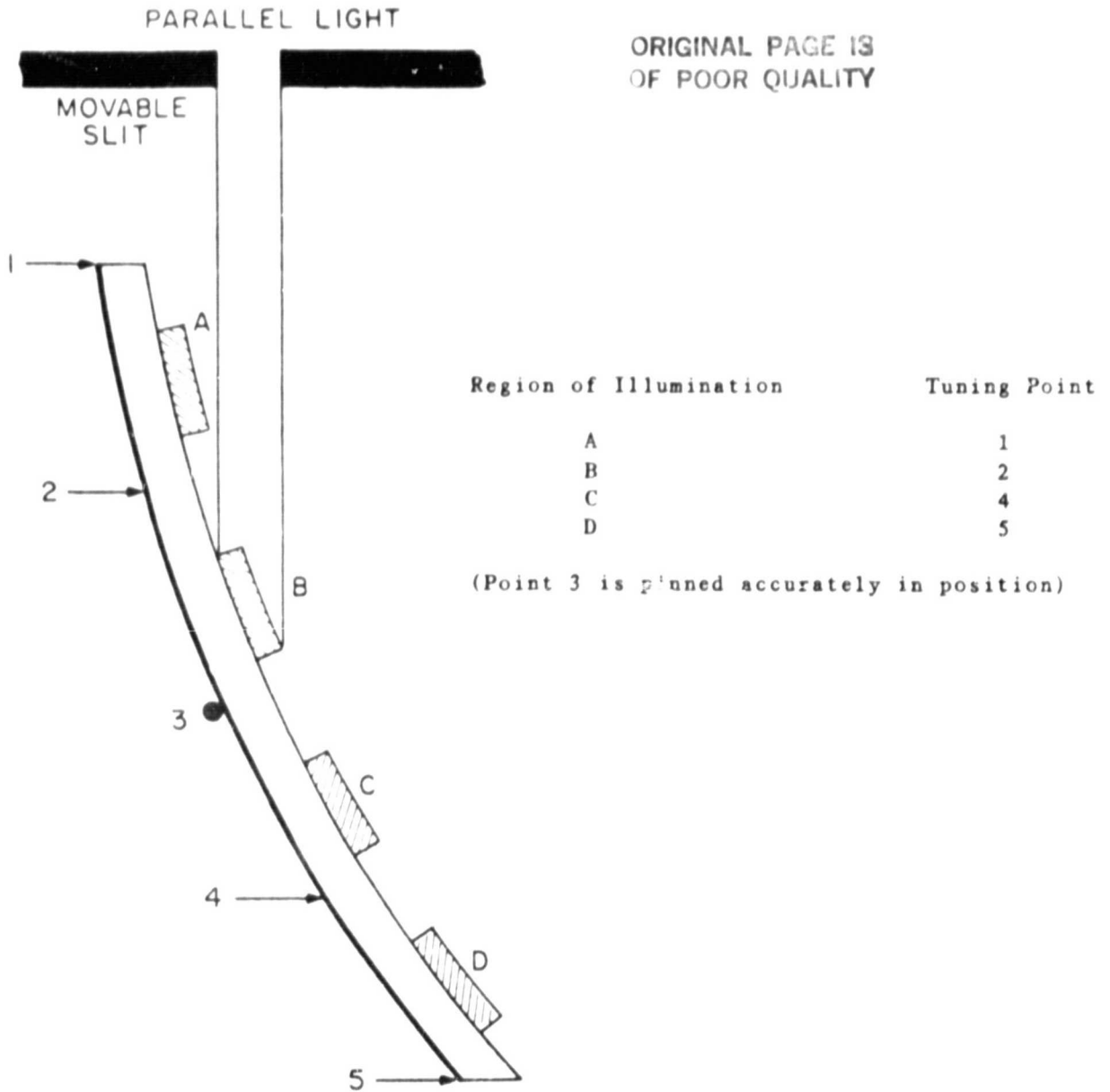


Figure 3-9

A schematic of the procedure for mirror figure formation which is performed in a parallel light beam. A slit is used to define the region of illumination on an individual plate and motorized controls are operated until the figure is acceptable. The tuning procedure is iterative so that the sequence of tuning shown is repeated typically three times.

position to an accuracy of 10^{-4} inches. Thus the region of the plate being illuminated is controllable to a high degree of accuracy. Farther along the

optical bench a set of 256-channel diode arrays ("reticons," manufactured by the EG and G Corporation) are mounted in the focal plane of the mirror. Light reflected from the mirror appears as a line image upon the reticons. Because of diffraction the width of the image can be wider than the open area of the slit. However, the centroid of the image is still determined by the average angular slope of the region exposed and is not affected by diffraction. The reticons are located at the top, middle, and bottom of the image. Their vertical position can be controlled with a motor drive for making additional readings along the line image.

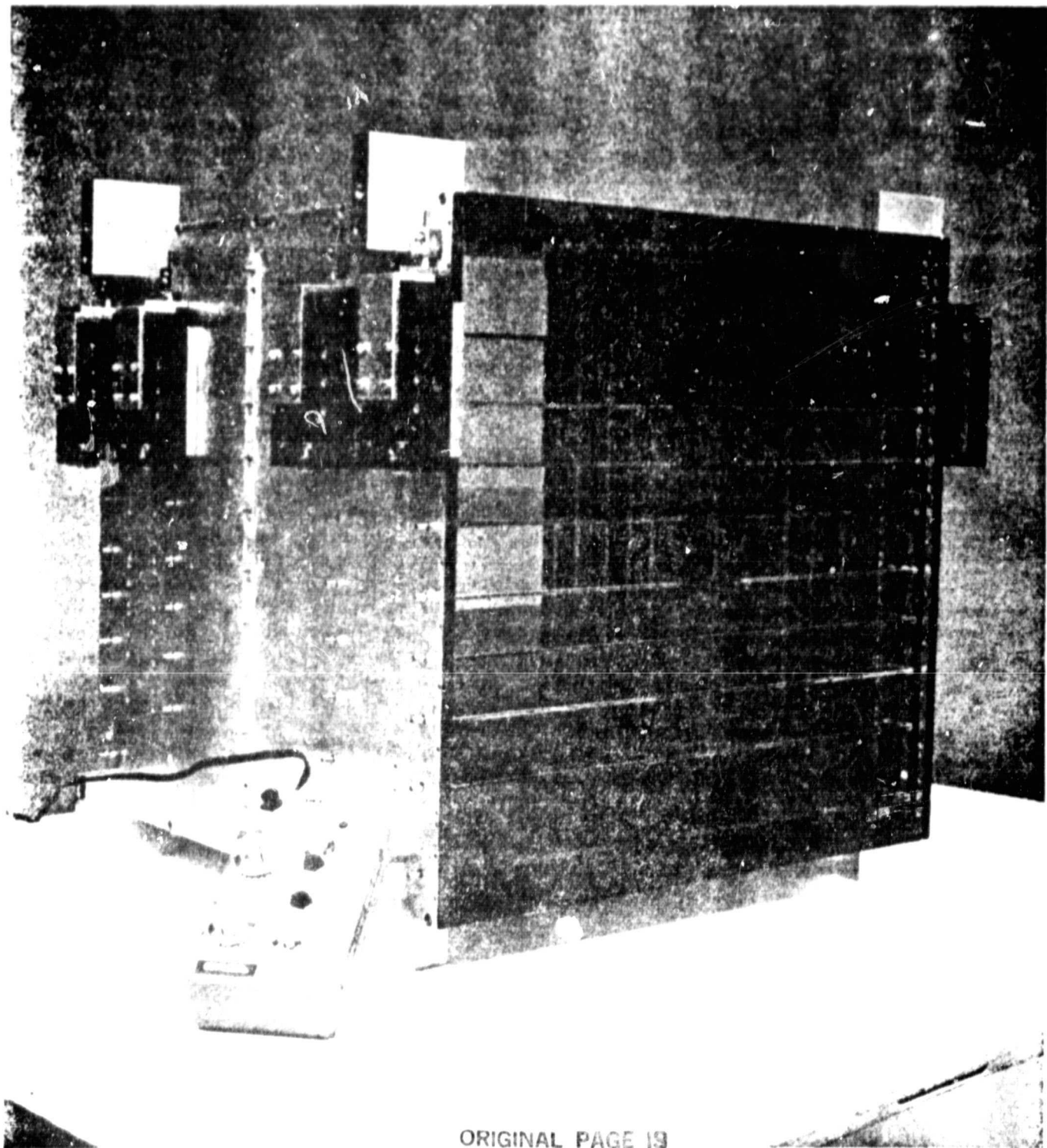
The adjustable points are controlled by a set of eight external micrometers driven by small linear motors. The precision of the micrometer system is about 0.1 microns, which far exceeds our requirements. Figure 3-10 is a photograph of a mirror box illustrating the placement of the motorized micrometers.

Outputs from the reticons are read into a microcomputer continuously, with updates at intervals of a few seconds. The three images are displayed on the screen along with their centroids. The tuning procedure consists of illuminating the plate in a prescribed sequence by controlling the slit position. By activating the micrometer motors the operator brings the centroid of the image as close to the central channel of the reticon array as possible. The process converges after three to four cycles of tuning or about one-half hour of time.

3.4.4 Performance Of The Mirror Brassboard

Using the methods described above we have constructed a brassboard X-ray mirror including both front and rear sections. The dimensions of the mirror are full scale. However, we have included only one out of three mirror plates, or 18 out of a maximum possible total of 54. This number is sufficient to verify the method at essentially all of the mirror positions from the outermost to the innermost plates. The average time required to tune a plate was 30 minutes, and a few additional minutes were needed to transfer the eight motor driven micrometers to the next plate.

The angular resolution of each plate is measured in visible light by constructing a histogram of the distribution of the centroids of images from parallel pencil light beams reflected from the plate at a large number of points. By plotting the distribution of image points as a histogram, we effectively reconstruct the mirror's point response in visible light. The angular resolution, as measured by this method, is also representative of the angular resolution in X-rays. X-ray scattering measurements made on float glass samples by us and others invariably find that material to be rather smooth on a scale of several angstroms.



ORIGINAL PAGE 19
OF POOR QUALITY

Figure 3-10

The front section of the LAMAR mirror brassboard which contains ten mirror plates, roughly one half of the full complement of plates. The rear mirror section (whose appearance is similar) is not shown. The mirror tuning pins and the motorized positioning stages used to form the mirror figure can be seen on the side of the mirror box.

In fact, float glass is often used as a standard of comparison in polishing surfaces of X-ray telescopes. Interferometric measurements, which examine the material on intermediate scales, do not reveal surface irregularities beyond what we detect in our assessment of the mirror brassboard by the methods described above.

Figures 3-11 and 3-12 show the angular resolution of the front and rear sections of the X-ray mirror brassboard. The differential and integral distributions of the pencil beam images are shown. For the front mirror the diameter of a circle which contains 50% of the intensity is 27.6 arcseconds. For the rear, it is 42.2 arcseconds. With two reflections occurring serially at grazing incidence, the two reflections are effectively independent and the two-dimensional angular resolution would be the geometric mean of these two numbers or about 34 arcseconds.

The angular resolution that we obtain is consistent with the intrinsic flatness of the float glass material as measured by two methods. One was an independent set of interferometric measurements made on 25 other plates from the same stock as the glass plates used in the fabrication of the brassboard. Those measurements characterize the flatness as being in the range 25 to 40 arcseconds diameter, consistent with the resolution of the mirror. The other measurements were normal incidence, auto-collimator scans of the telescope's plates prior to insertion in the mirror box. Those measurements corroborate the performance of the front and rear mirrors. The conclusion is that the accuracy of tuning was finer than the flatness of the material. The superiority of the front mirror with respect to the rear is a consequence of its having received the flatter glass plates from the lot. It follows that, had we been able to select from a larger stock and reject the inferior material, the angular resolution of the other mirror would have been equal to the front. For the flight mirror we would select the plates from a stock that is 2 to 3 times larger than the number to be used. On this basis it is reasonable to expect the angular resolution to be better than 30 arcseconds.

Because scattering from float glass is small, the angular resolution of LAMAR will be essentially independent of energy. The behavior of the Einstein Observatory's mirror was quite different in that scattering affected an increasing fraction of the power at higher energy. In fact, the 50% power diameter of LAMAR is expected to be smaller than that of the Einstein mirror above 4 keV.

3.4.5 Materials And Machining

After the glass is received from the supplier, each plate is examined for flatness with a large area Fizeau-type interferometer. The interference pattern between the plate and a reference optical flat is displayed on a TV monitor. An acceptable plate is one where the density of fringes is fewer than nine per inch. Experience with the LAMAR mirror brassboard indicates that about half of

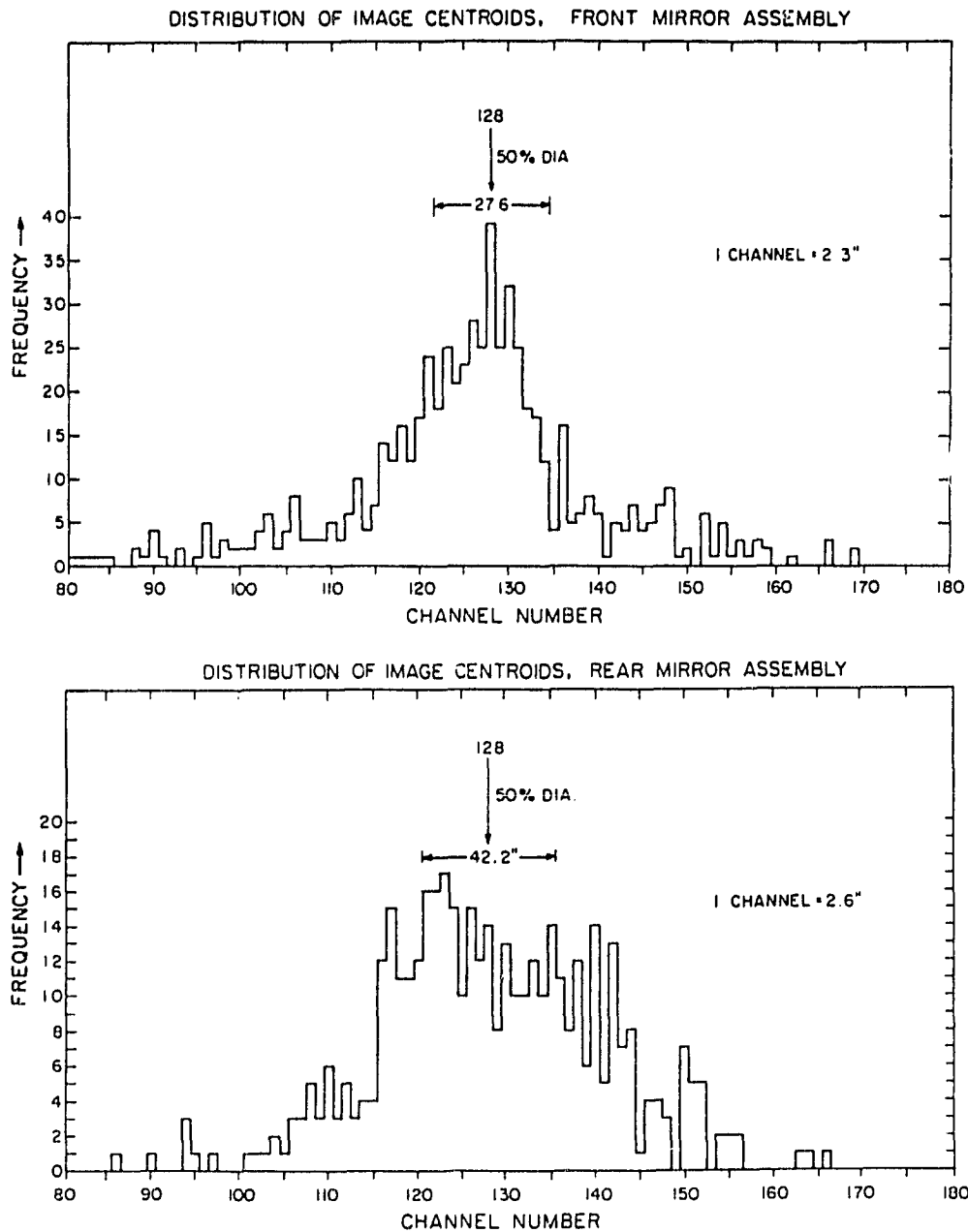


Figure 3-11 The distribution of image centroids obtained from the optical slit scans after each plate was epoxied into position. The integrated results from all plates in the front and back mirror assemblies are shown separately. We obtain a 50% power diameter of 28 and 42 arcseconds for the front and back assemblies respectively. These results are consistent with the measured slope errors of the plates. The front mirror results are superior because the best plates were selected for use there, and the remainder left for the back mirror assembly.

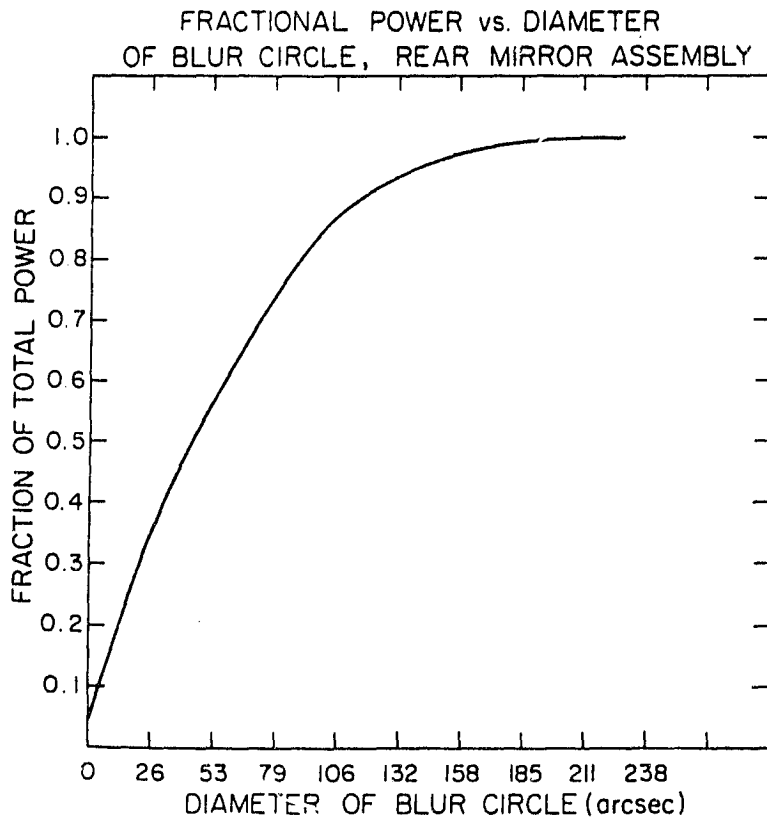
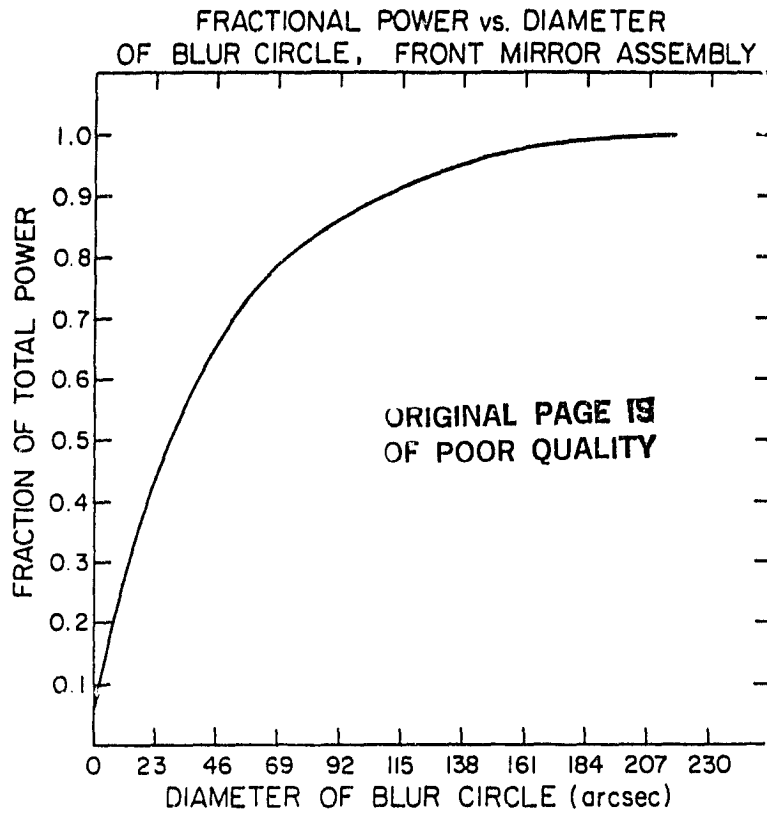


Figure 3-12 The same data presented in Figure 4-5, but in an integral as opposed to differential form.

the plates are acceptable. A side panel in Figure 3-8 shows the interference pattern of a plate that is included in the mirror brassboard.

The process of figure formation begins with a procedure carried out on titanium alloy stock (5 mil) that has been cut into sheets which match the area of the glass plates. The titanium sheets are rolled into springs with small radii of curvature. When a titanium spring is bonded to a flat glass plate, the composite material assumes a larger radius of curvature which is approximately equal to that of the average radius of curvature of a parabola of the mirror. By varying the initial radii of curvature of the titanium springs, we can make composites that cover the full range of average radii of all the parabolas of the mirror. The initial radii of curvature vary from a few inches to many feet. This process is illustrated in a side panel of Figure 3-8.

Several machining operations occur in parallel with the process described above. The four side plates which give structural integrity to an assembly of mirror plates are made by conventional procedures. The top and bottom plates contain a pattern of holes, there being five holes for each mirror plate. The function of these holes is to allow extender rods bonded to the plates at five points along the top (bottom) edge of the mirror plate to pass through with about .05 inches of clearance. No special precision is needed in the location of these holes. We also fabricate ten "U" shaped channel clips for each plate, with extender rods measuring .5" by .01" diameter attached. They are shown in a photographic side panel of Figure 3-8.

3.4.6 Interactive Tuning

Figure 3-13 is a series of reticon readings for a particular plate shown together with the three centroids of the light distribution as calculated by the microcomputer. The central position is channel 128, and each channel corresponds to 2.3(2.6) arcseconds for the front(rear) mirror. Panels a-d refer to the same region of the plate following successive adjustments to that region and others. Panel e is the final condition following the last adjustment of the plate. Panel f is the reticon readings when the entire front mirror is illuminated by the light beam.

When the interactive adjustments are complete the figure of the plate is measured by determining the centroids of light reflected from many points on the plate. The motor driven slit is moved in steps of 20 mils through the projected area of the plate. Seven samples are taken along the vertical direction by varying the height of the reticons. For the outermost plate which has the largest projected area, over 100 readings are taken. A histogram of these image positions is indicative of the angular resolution of the plate. Although these measurements are made in visible light, they also represent the plate's X-ray performance. It has been established through X-ray measurements that scattering from float glass is very low and that deviations from flatness occur on a scale that affects visible light imaging properties in the same way that it does the

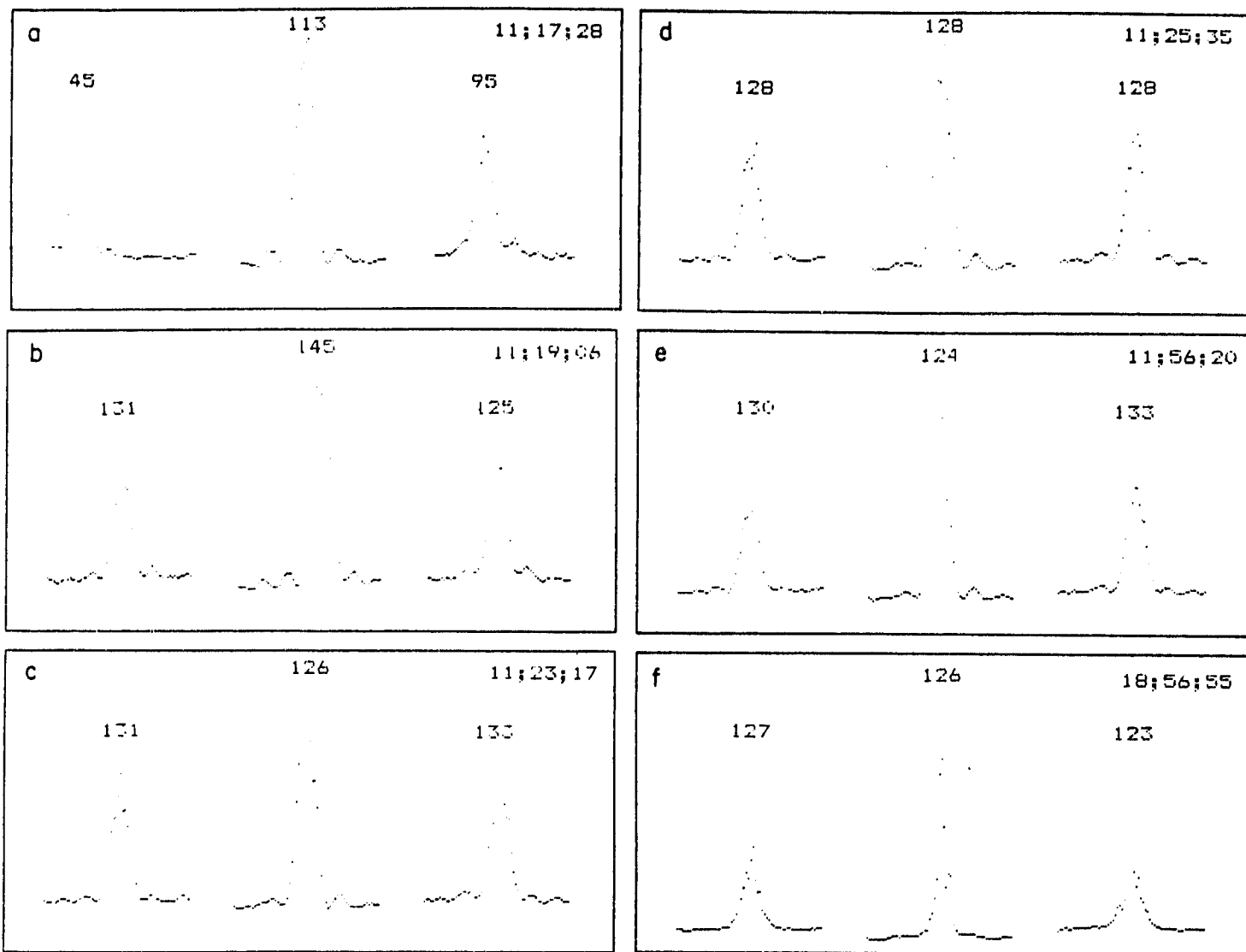


Figure 3-13 Series of reticon readings as figure of plate is tuned interactively. Numbers above the slit denote the centroid of the image as determined by the microcomputer. The on axis position is Channel 128, and one channel corresponds to 2.3 arcseconds. The time is shown in hrs:min:sec. Panel a is taken near the start of the tuning process. Panels b, c, and d show the progressive improvement that occurs when the plate is adjusted by exercising the two central points nearest the region of illumination. Panel e shows the final condition at that point when all adjustments on that plate have been completed about one-half hour later. Panel f, taken two days later, refers the image of the entire front mirror brassboard which contains 10 plates.

X-ray properties. When the tuning process is complete the extender rods are permanently bonded to the mirror box with epoxy, and the micrometers are transferred to another plate.

4.0 CONCLUSIONS

In this course of this study we addressed the following four areas:

- a) Thermal
- b) Spectroscopy
- c) Pointing System
- d) Mirror Module Performance

Our purpose was to identify the most important questions in each of the four areas, devise a solution and produce a design that could be implemented when the LAMAR experiment is developed. We summarize the results in each of the four areas.

(a) Thermal

We completed one of the most important aspects of the thermal design. A thermal pre-collimator concept was designed and tested. Modeling tests indicate that the concept would succeed in keeping temperature gradients in the mirror assembly to acceptable levels. More details remain to be worked out in the mirror itself such as the need to identify a metal foil whose coefficient of thermal expansion matches that of the glass optimally. In summary, no fundamental unsolvable problems were uncovered.

(b) Spectroscopy

Our study indicates that a moderately high resolution, high throughput dispersive spectroscopy capability could be added to LAMAR as a part of a refurbishment after the initial flights of the instrument take place with imaging measurements. The spectroscopy feature is added by mounting a rigid box containing a nested array of blazed reflection gratings to the front of the mirror assembly. The system would have two orders of magnitude greater effective area than the objective grating spectrometers of the Einstein Observatory and EXOSAT.

(c) Pointing System

With new information available on the pointing system and refinements in design of LAMAR there is complete compatibility with the pointing system of the Cirrus experiment. Use of the pointing system is highly beneficial as it results in much more efficient utilization of the observing time. With the increased efficiency of the pointing system we felt that it was no longer necessary to include the provision for easy expandability of LAMAR. In effect the pointing system was equivalent to having a larger instrument. By dropping the provision for expandability we were able to significantly reduce the cost of building LAMAR.

(d) Mirror Performance

The most effective means of stiffening a float glass plate against elastic distortions proved to be bonding a pre-curved metal foil over the entire surface of the glass. The bond material was then in its approximately correct radius of

curvature. Tuning was then only a matter of applying very small changes to the figure of the material.

The angular resolution performance of the mirror module prototype was measured to be 30 seconds of arc diameter for 50% of the power. This performance was ascertained by a combination of tests in visible light and x-rays. The x-ray tests apply to size scales below 1 centimeter and the visible light tests to scales above 1 cm. The limiting factor is believed to be the flatness of the glass. With the ability to select the glass for flatness as we would be able to do in a large purchase when building LAMAR mirrors for flight we expect that the resolution would be even better. There does remain the question of which metal alloy does match the coefficient of thermal expansion of the glass best? Direct measurements should be carried out on several sample glass-metal bonded materials to answer that question.

APPENDIX I

LAMAR THERMAL PRECOLLIMATOR: PROOF-OF-CONCEPT MODELS

THERMAL-VACUUM TEST REPORT

CONTENTS

| SECTION | | Page |
|---------|---|------|
| | INTRODUCTION | 1 |
| | BACKGROUND--THE LAMAR INSTRUMENT | 3 |
| | PRECOLLIMATOR DESIGN CONCEPTS | 5 |
| | Vignetting: | 5 |
| | Thermal Performance Considerations: | 7 |
| | TEST METHOD AND TEST ARTICLE | 11 |
| | TEST CONFIGURATION AND INSTRUMENTATION | 15 |
| | MODELING OF TEST CONFIGURATION, PREDICTIONS | 16 |
| | CONCLUSIONS | 18 |

FIGURES

| | | |
|----------|---|----|
| FIGURE 1 | LAMAR Instrument--Exploded View | 2 |
| 2 | LAMAR Basic Array Subassembly (BAS) | 2 |
| 3 | Aperture Locations of On-axis Rays Reaching Focal Plane | 4 |
| 4 | Aperture Locations of $\pm 30'$ Off-axis Rays Reaching Focal Plane | 4 |
| 5A | LAMAR Thermal Precollimator Schematic | 6 |
| 5B | Precollimator Configuration Assumed for Thermal Model | 6 |
| 6 | Thermal Model of the Thermal Precollimator | 8 |
| 7 | Thermal Performance of LAMAR Thermal Precollimator Configurations | 9 |
| 8 | Sketch of Test Article | 10 |
| 9 | Subassemblies of the Test Article | 12 |
| 10 | Assembled Test Article and Installation in Chamber | 14 |

TABLES

| | | |
|---------|--|----|
| TABLE 1 | LAMAR Precollimator Thermal-Vacuum Test Sequence . | 15 |
| 2 | Comparison of Test Results and Predictions | 17 |

INTRODUCTION

The Large Area Modular Array of Reflectors (LAMAR) instrument¹ is to be a Shuttle-launched X-ray observatory to carry out cosmic X-ray observations for periods of a few days to several years. A primary characteristic of LAMAR is its large telescope aperture area, which potentially represents a severe requirement for thermal control power to maintain temperature. A precollimator that would pass incident X-rays but restrict thermal loss has been proposed as a major element of a LAMAR thermal control system. (The term precollimator refers to an assembly of parallel cells of roughly rectangular cross-section, analogous (though not identical) to honeycomb core material. Its purpose is to reduce thermal radiation through the assembly by restricting radiative viewfactors, but allowing collimated X-rays to pass.)

This report discusses an analytical design study and proof-of-concept thermal-vacuum test of the LAMAR insulating precollimator. The test results confirmed the predictions of the analytical models, which show that reduction of a factor of three or more in radiative heat loss from the telescope apertures is possible with the proposed precollimator.

¹The discussion of the LAMAR instrument contained in this report is based upon a conceptual design developed during the period 1981-1983, and described in an Experiment Requirements Document and Instrument Development Plan submitted to Goddard Space Flight Center in that period. The current design concept for mounting on a CIRRIIS pointer, as described in 1984 updates to those documents, differs in some mechanical details. However, the thermal design concept has changed very little, so that the information presented herein remains valid.

ORIGINAL PAGE IS
OF POOR QUALITY

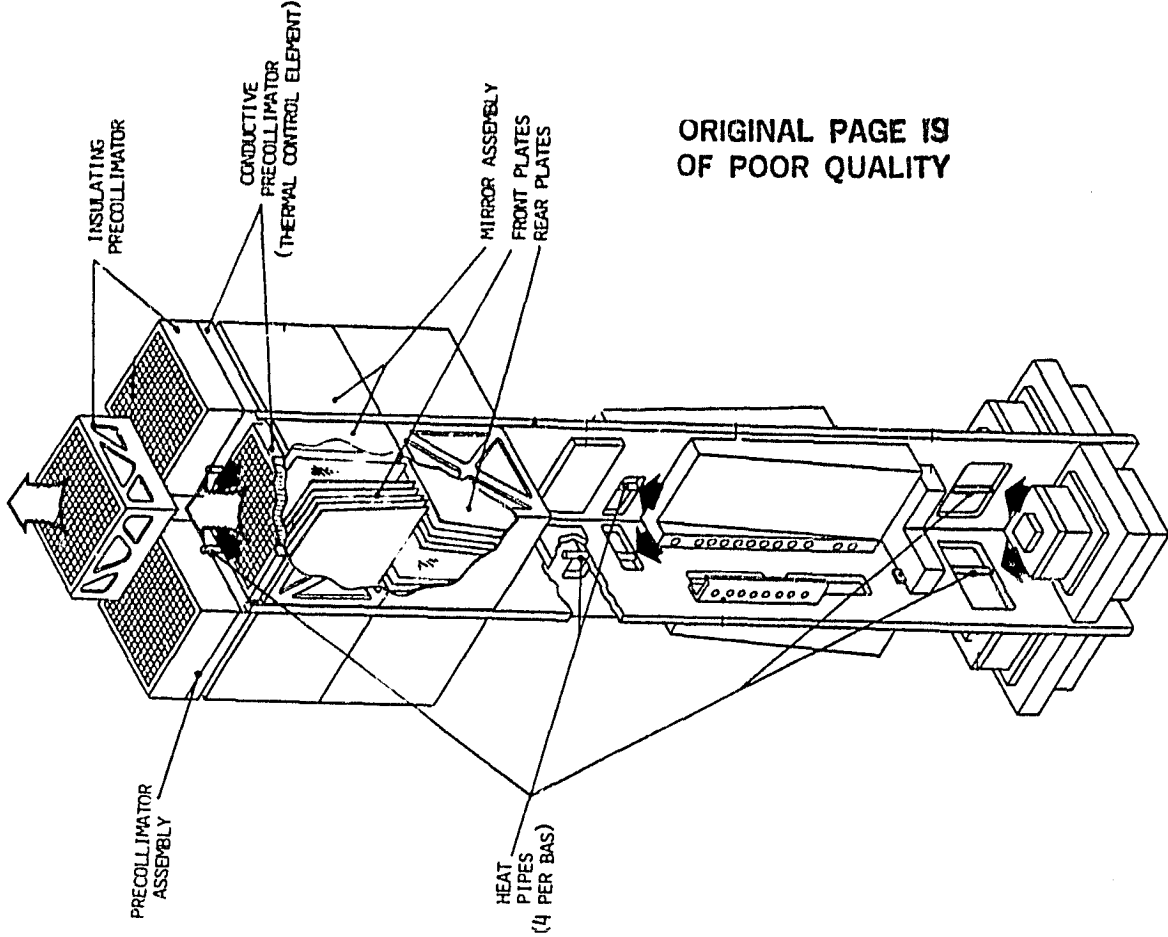


Figure 2. LAMAR Basic Array Subassembly.

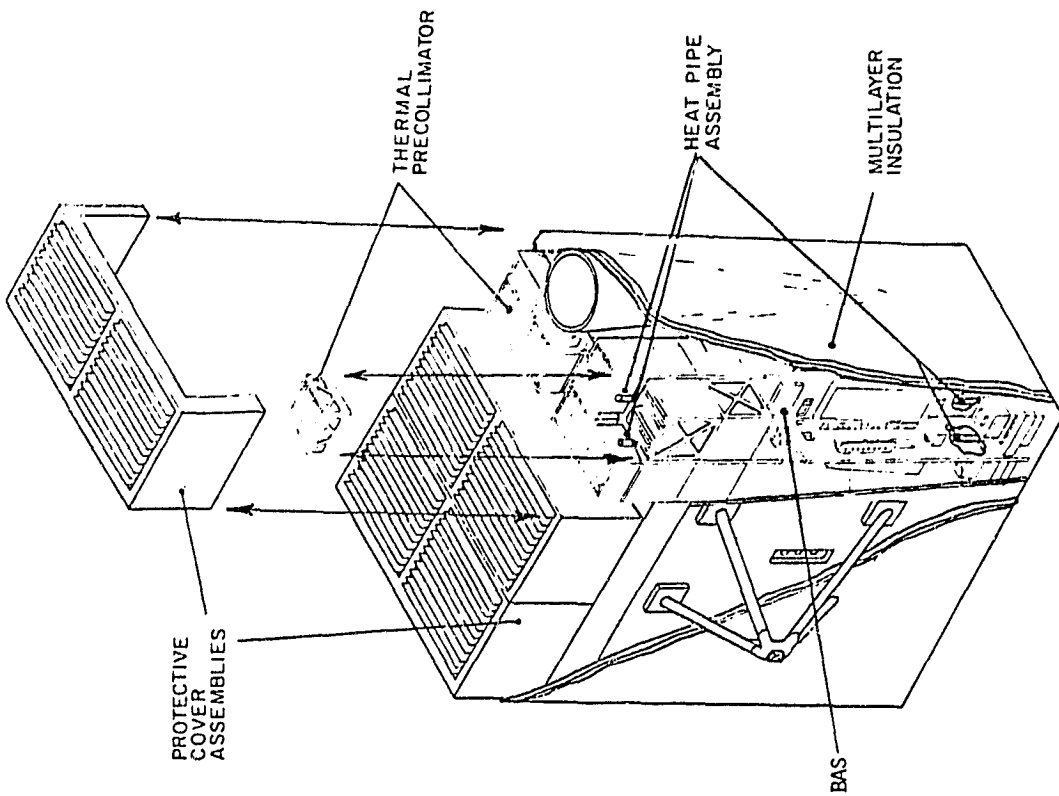


Figure 1. LAMAR Instrument - Exploded View.

BACKGROUND--THE LAMAR INSTRUMENT

The LAMAR instrument (Figure 1) consists of a parallel array of grazing incidence X-ray telescopes that focus incident X-rays on individual detector assemblies. Telescopes, detectors, and their associated electronics are functionally, physically, and electrically organized into groups of four. Each module of four telescope mirror assemblies, detectors, thermal precollimators, and detector processing electronics is a separate functional and physical entity. This module (shown in Figure 2) is designated a Basic Array Subassembly (BAS) and is the "building block" from which a LAMAR array of arbitrary size is constructed.

Each BAS has a protective cover to prevent focussing of the sun on the detector during a solar transit. The Nested Parabolic Plate Mirror Assembly (Figure 2) consists of two orthogonal sets of nested glass plates, coated with nickel or gold to enhance X-ray reflectivity. Each plate is bent into approximately a parabolic shape, determined so that the entire set of plates brings an incident parallel beam of X-rays into a common focus.

A thermally-conductive precollimator, separating the telescope apertures from space, is the primary control surface of the BAS. Four axial heat pipes transport detector and processor power from the focal plane region forward to this precollimator, from which it is radiated to space. An additional insulating precollimator controls the effective radiative properties of the aperture so that full internal power produces the desired operating temperature in the hottest orbital orientation. Active thermal control provides additional power to maintain temperature in colder orientations, and the tight coupling of detectors and precollimators by the heat pipes ensures close control of detector temperatures. Total dissipation capability of the aperture area would be about 37 watts/ft² without the insulating precollimator.

Figure 3: Aperture Locations of On-Axis Rays Reaching Focal Plane
(One Quadrant of Mirror Shown)

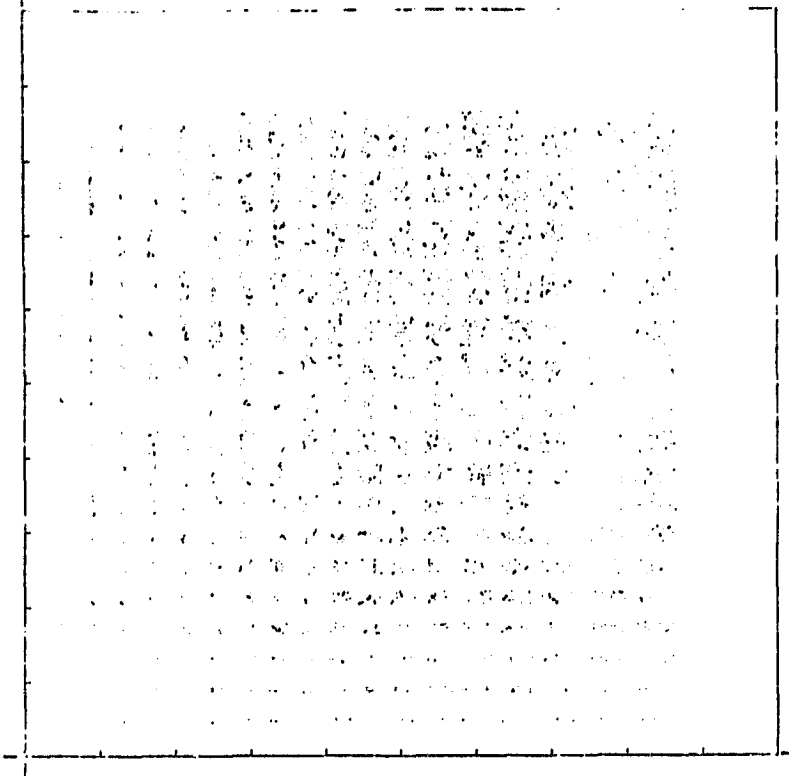
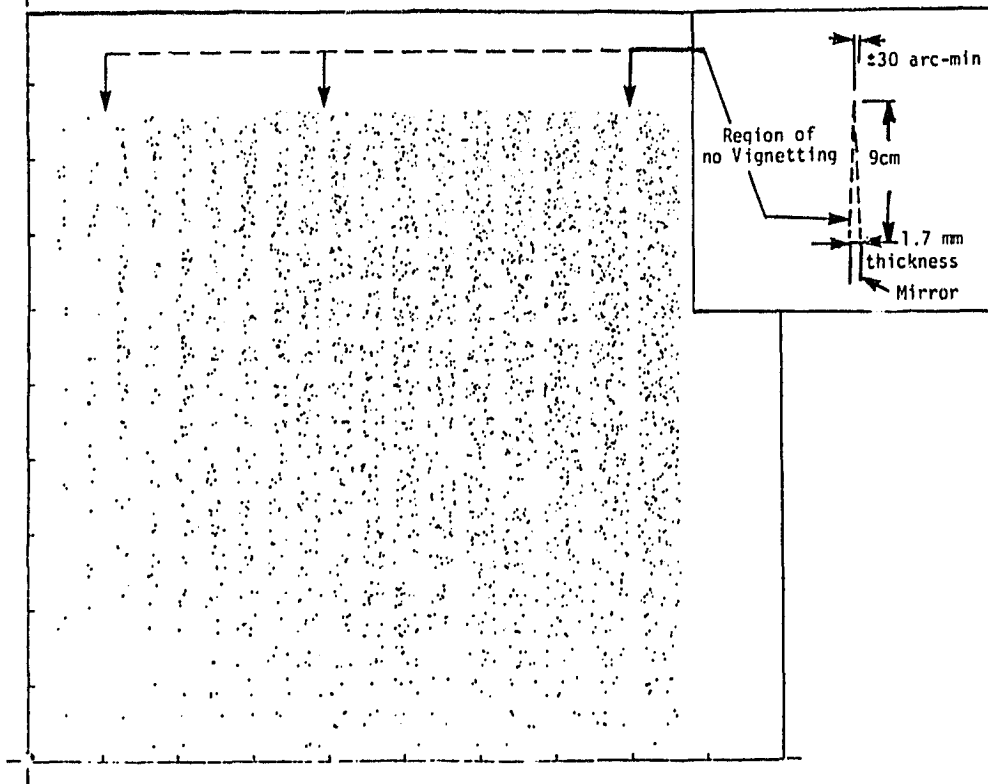


Figure 4: Aperture Locations of 30° Off-Axis Rays Reaching Focal Plane



PRECOLLIMATOR DESIGN CONCEPTS

The forward ("insulating") section of the precollimator, along with the protective cover, controls radiative heat loss from the conductive precollimator section covering the aperture by restricting its view factor to space. Heat flow through test models of possible configurations of this forward section and the protective cover were measured in a proof-of-concept thermal-vacuum test, and compared with predictions obtained using mathematical models. This section describes the precollimator configurations used in the test, and the results of the design study that led to their selection.

There are three major constraints on precollimator design:

1. There should be minimum vignetting of incident X-rays
2. The aperture should radiate full experiment power (15-25 watts/ft²) at 60 degrees to the sun (incident energy about 65 watts/ft²)
3. Thermal control power should be reasonable (about 5 watts/ft²) when viewing deep space.

Vignetting:

The first constraint requires that precollimator and protective door elements be aligned with frontal elements that do not form part of the effective area (such as mirror edges and the BAS structure) insofar as possible within thermal performance requirements. Figure 3 is a plot of coordinates at the mirror entrance aperture, generated by a Monte Carlo model, of on-axis X-rays that reach the focal plane (one quadrant of the telescope is represented). A grid pattern of spaces indicates the projections of mirror edges on the aperture; on-axis rays arriving in these regions will not reach the focal plane. Figure 4 is a similar plot for X-rays arriving at ± 30 arc-minutes off-axis. In this case the edges of only the front mirror set represent "dead areas." Assuming 1.75mm mirrors, regions of no vignetting for 30 arc-minute x-rays have triangular cross-section (see Figure 4, inset) 1.75mm wide at the base and about 9cm high. In addition, the spaces between the mirror quadrants are inactive and can be used without impact. A bias toward long rectangular cells, having precollimator elements located within the dead areas, is clear from Figure 4.

LAMAR THERMAL PRECOLLIMATOR SCHEMATIC

ORIGINAL PAGE IS
OF POOR QUALITY

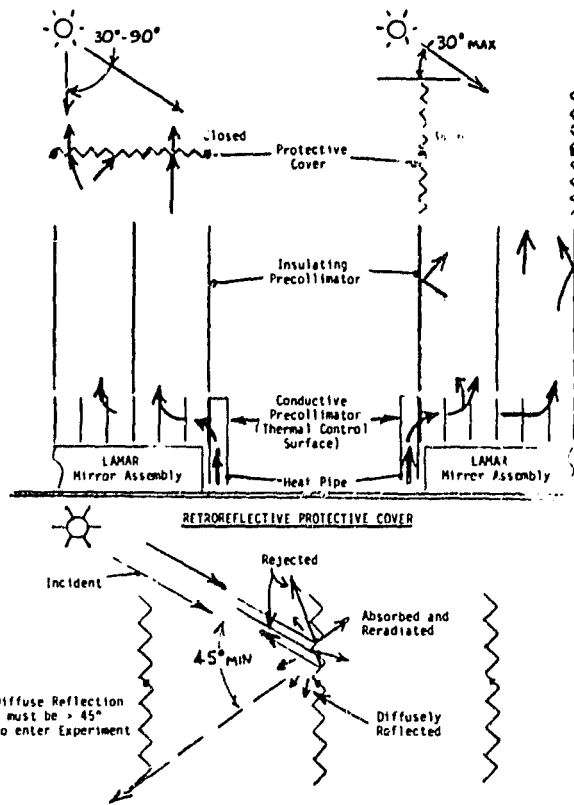


Figure 5a. LAMAR Thermal Precollimator Schematic.

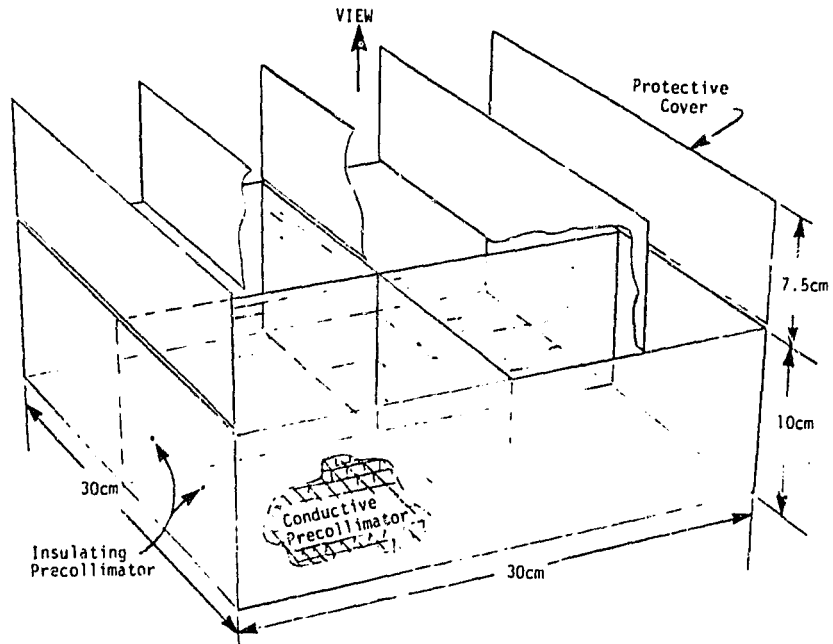


Figure 5b. Precollimator Configuration assumed for Thermal Model.

Thermal Performance Considerations:

The second constraint implies that the precollimator/protective cover combination must reject enough of the solar load at 60° incidence to permit full experiment power to be radiated, so that thermal control may be maintained. Using either diffuse or specular surface coatings will cause at least half the incident load to be scattered or reflected into the precollimator; the aperture cannot radiate this much power plus experiment power (>50 watts total) at the desired operating temperature. Most of the incident load must therefore be rejected to space without being absorbed, which will require using a surface with retroreflective properties for the protective cover. One possible configuration has a sawtooth cross-section with specular surfaces as illustrated in Figure 5A. The present study indicates that this type of surface will fulfill the design constraint. However, the effect of such a surface on precollimator thermal performance can only be approximated mathematically. A reasonably accurate model of such a cover was included as a part of the test article so that its effects could be measured.

The third design constraint implies that the precollimator must reduce aperture loss by approximately a factor of 1.5-2.5 when facing space, from the blackbody value of 37 watts/ft² to about 15-25 watts/ft². (The range is needed at this preliminary stage because exact values of experiment power and other thermal control parameters are not known precisely.) A design study using a thermal mathematical model of the precollimator predicted thermal performance of precollimators with different sizes of square and rectangular cells, with and without the protective cover, for extremes of incident solar loads. Figure 5B is a sketch of the basic configuration assumed for a single telescope module. The principal elements shown are the "box" around the perimeter, a cruciform aligned with the inactive region in the center of the telescope, and a protective cover as shown in Figure 1. Additional square or rectangular cells were assumed to fill the quadrants formed by the cross and box. Radiation from the aperture to space at a temperature of 20°C was calculated for each configuration and compared with the case for no precollimator.

Figure 6 shows the subdivision of a typical cell in the thermal model. Each of the levels of the cell and cover is assumed to view the simulated aperture and space, and the aperture views space directly through the open area. Effects of conduction (although small) were included. The same model was used, with modifications, to represent test conditions; this is discussed further on page 16.

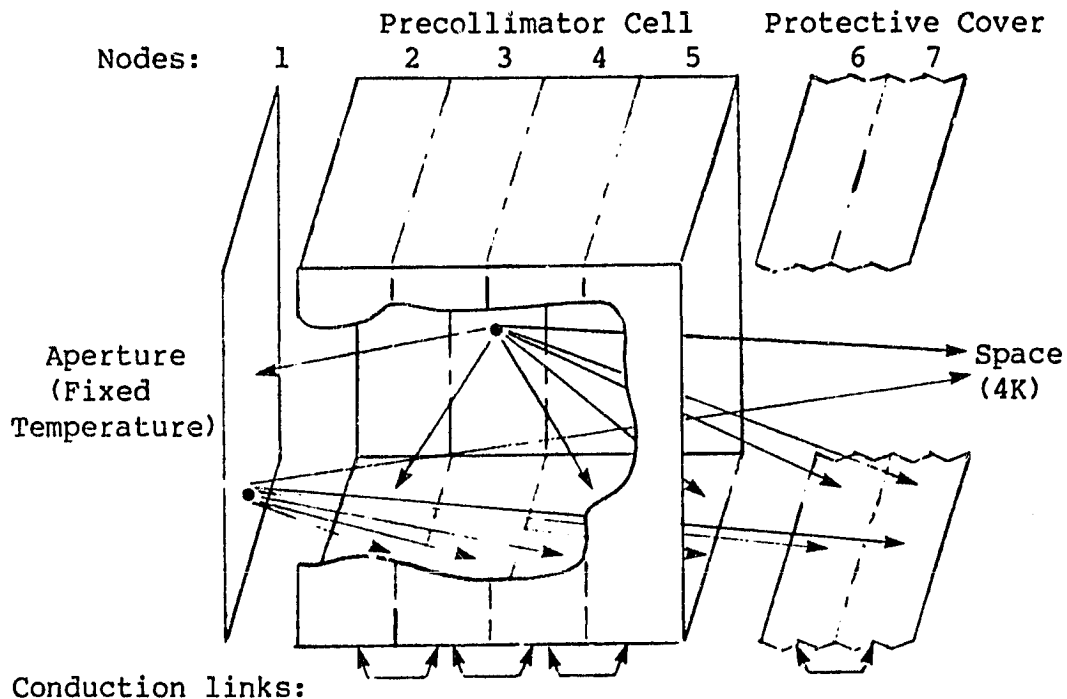
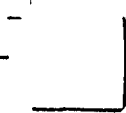
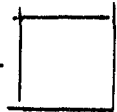
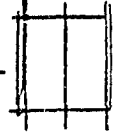

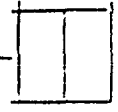
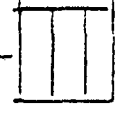
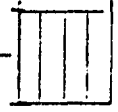
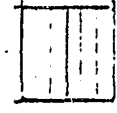
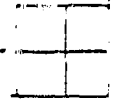
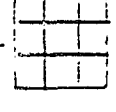
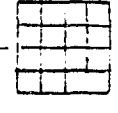
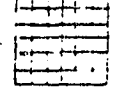
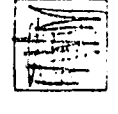


Figure 6. Thermal Model of the Thermal Precollimator

Results are shown in Figure 7. A sketch of one quadrant is included for each case. The "effective emittance" column is the fraction of the "no precollimator" loss for each case. It is evident that the case of the box and protective cover alone reduces loss by about a factor of 1.5, to 24 watts, and that five slats coincident with mirror edges (forming six rectangular cells) reduces loss by about a factor of three, to 13 watts. Use of the cross alone would not vignette the aperture at all beyond the effects of the protective cover, and the five-slat case would result in only a small amount of vignetting. These cases bracket the likely design conditions, and have been selected for the proof-of-concept test. It should be noted that square cells, which would have much greater vignetting effect, provide only a very small advantage in thermal performance over rectangular cells. Square cells would probably be considered for use only in a demanding mission which has very tight power constraints.

FIGURE 7

THERMAL PERFORMANCE OF LAMAR PRECOLLIMATOR CONFIGURATIONS

| <u>Configuration</u> | <u>One Quadrant</u> | <u>Facing Space Radiative Loss (Watts)</u> | <u>Effective Emittance</u> | <u>60° to Sun Radiative Loss (Watts)</u> |
|--------------------------|---|--|----------------------------|--|
| No Precollimator | | 37 | 1.0 | |
| Frame Alone |  | 29 | 0.77 | |
| Cross in Center |  | 24 | 0.64 | |
| Cross+Protective Cover |  | 21 | 0.55 | 17 |
| Protective Cover Alone |  | 24 | 0.64 | 20 |
| Cross + 1 Slat/Quadrant |  | 20 | 0.54 | |
| Cross + 2 Slats/Quadrant |  | 18 | 0.48 | |
| Cross + 3 Slats/Quadrant |  | 16 | 0.42 | |
| Cross + 5 Slats/Quadrant |  | 13 | 0.34 | |
| 4 Cells/Quadrant |  | 18 | 0.49 | |
| 9 Cells/Quadrant |  | 15 | 0.41 | |
| 16 Cells/Quadrant |  | 13 | 0.35 | |
| 25 Cells/Quadrant |  | 12 | 0.32 | |
| 49 Cells/Quadrant |  | 10 | 0.26 | |

ORIGINAL PAGE IS
OF POOR QUALITY

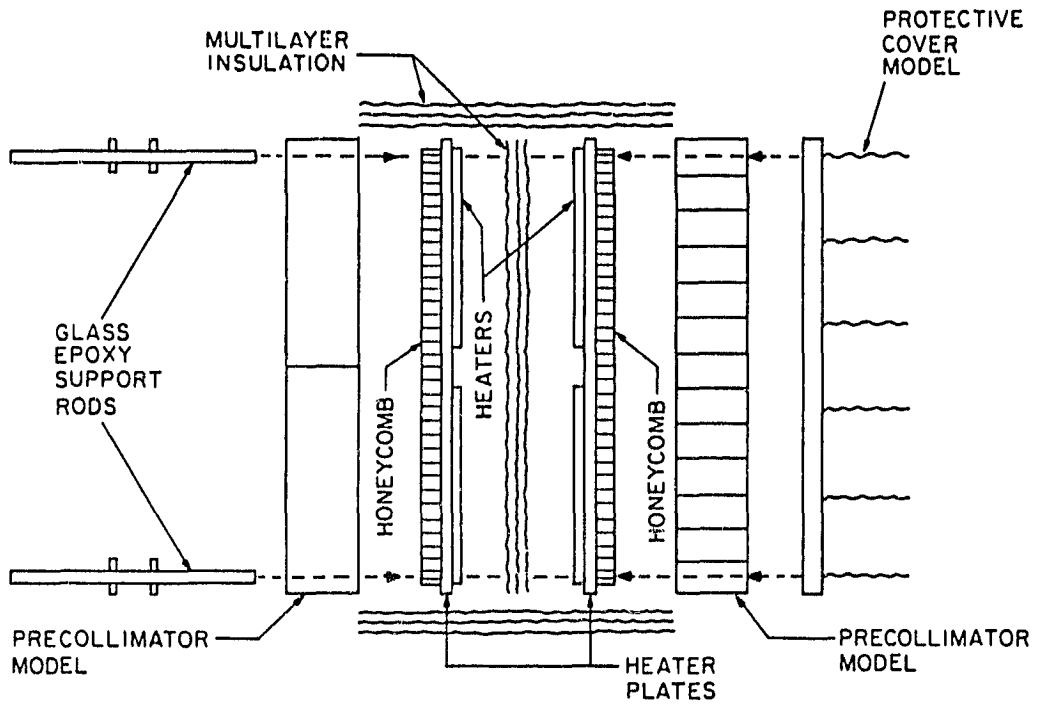


Figure 8. Sketch of Test Article.

TEST METHOD AND TEST ARTICLE

A calorimetric thermal-balance test method was selected to verify the performance of the precollimator. This type of test requires accurate correspondence of the physical test model to the analytical model used to predict performance. A high-emittance plate simulating the telescope aperture was maintained at a measured temperature by electrical heater in a thermal-vacuum chamber with cryogenically-cooled walls. Models of various precollimator configurations were placed in front of the plate, and electrical power measured at equilibrium conditions.

The accuracy of such an absolute measurement is affected directly by uncontrolled losses and uncertainty in emittance of the heater plate. Particular care was taken to minimize these effects. In particular, losses from the inactive side of the heater plate were eliminated by testing two models simultaneously in a back-to-back mode, similar to that used in the ASTM-C177 guarded hot plate thermal conductivity measurement procedure. This method is self-guarding for back losses because of the virtual adiabatic surface created by the symmetrical configuration. Edge losses could not be guarded because of the large temperature gradient in the precollimator models; multilayer insulation was used to minimize these edge losses.

Figure 8 illustrates the back-to-back test article configuration. Kapton-insulated foil heaters cemented to the back surface of quarter-inch aluminum comprised each heater plate. A quarter-inch thickness of aluminum honeycomb was cemented to the front (radiating) surface simulating the telescope aperture and the entire surface sprayed with black urethane paint. The radiating cavity effect of the conductive honeycomb assured a surface having emittance near unity. A multilayer insulation blanket was placed between the heater plates to improve thermal isolation between the two test sections. The heater plates and blanket were assembled with threaded glass-epoxy rods and nylon nuts and washers at each corner; the rods also were used to secure the precollimator models to the heater plates.

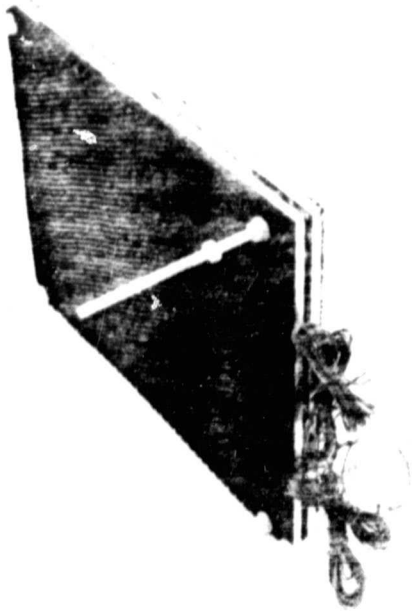


Figure 9A. Heater Plate Assembly.

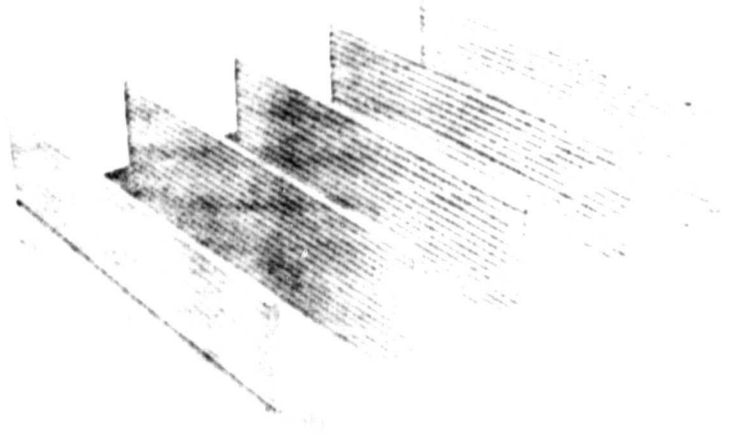


Figure 9B. Protective Cover Model.

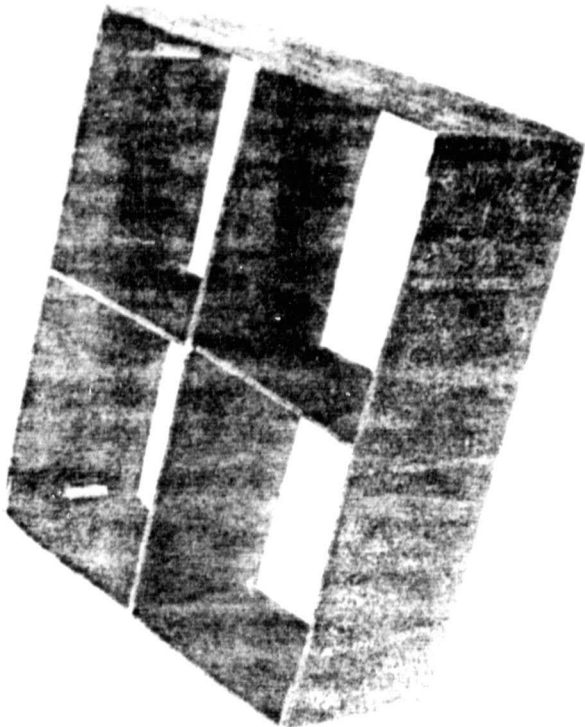


Figure 9C. 4-Cell Precollimator Model.

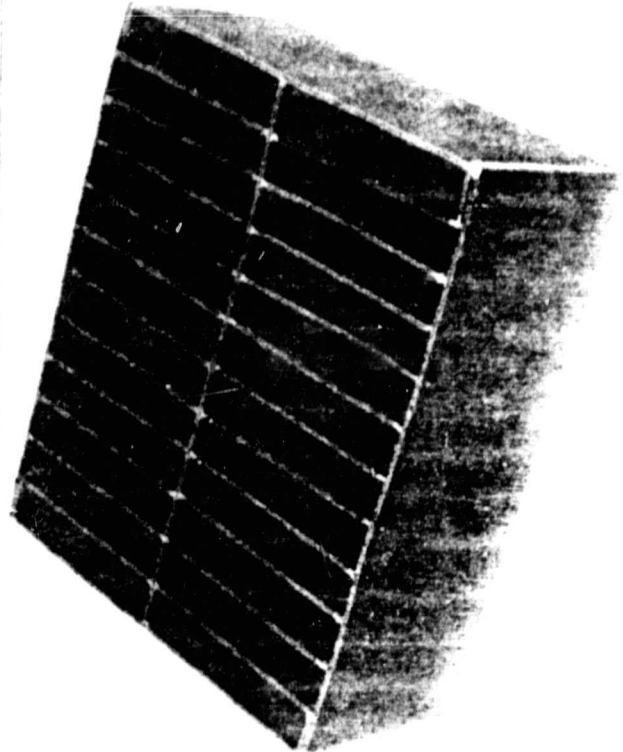


Figure 9D. 24-Cell Precollimator Model.

Figure 9A shows the two heater plates and blanket assembled and ready to receive the precollimator models. The precollimator models were constructed of eighth-inch polyurethane foam, lightly-impregnated with epoxy for structural rigidity. Foam was chosen primarily for low thermal conductance and for its irregular surface characteristics, simulating closely the Lambertian surface assumptions of the analytical thermal model. Figures 9B and 9C show the four-cell (cruciform) and 24-cell test models. These models were assembled in a way that permitted selection of alternate test configurations by removal of internal structure. Thus, the open configuration was produced by removing the cruciform from the four-cell model, and a 12-cell model resulted from taking internal slats from the 24-cell unit.

The protective cover model, shown in Figure 9D, was constructed of copper foil, covered with Teflon tape to produce a high-emittance surface. The cover model was supported by the glass epoxy rods in front of either precollimator model as needed. A multilayer insulation blanket of aluminized Mylar and Dacron scrim surrounded the assembled test article to control heat losses from its perimeter.

Twenty-one copper-constantan thermocouples were installed to indicate test plate and precollimator model temperatures. Figures 10A and 10B show two views of the assembled test articles before the first test. The protective cover model is installed in front of the 24-cell precollimator model, and the opposite side contains the four-cell cruciform model. The perimeter blanket and the thermocouple and power cables can be seen in the figures.

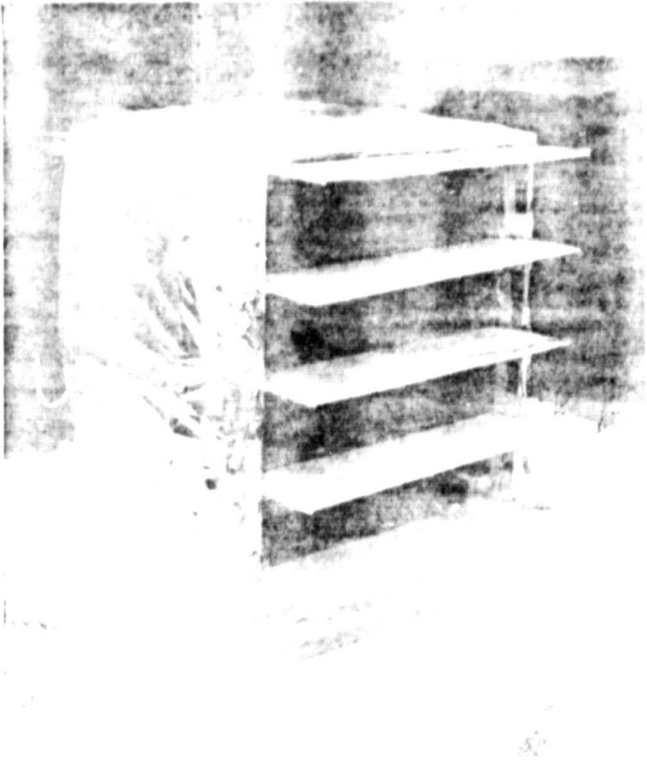


Figure 10A. Test Article, 24-Cell Side.

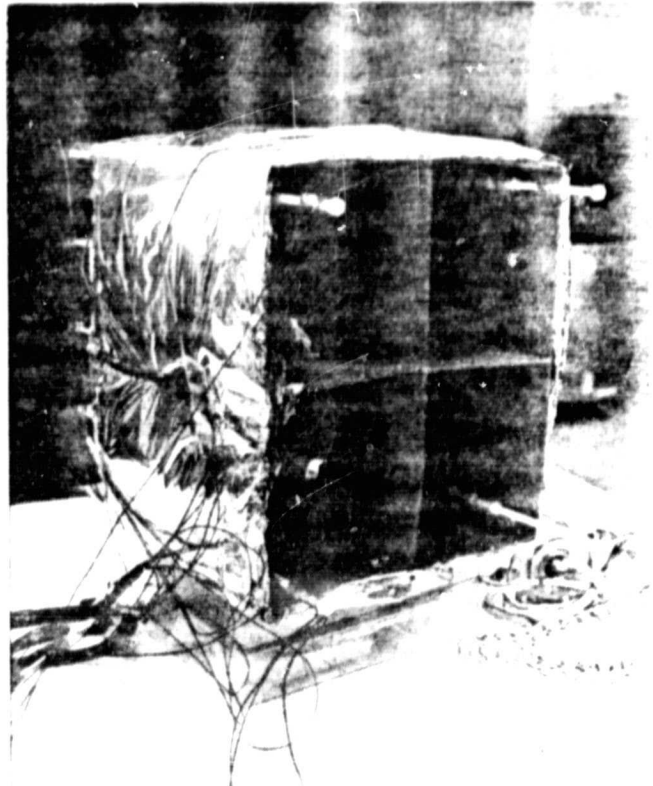


Figure 10B. Test Article, 4-Cell Side.

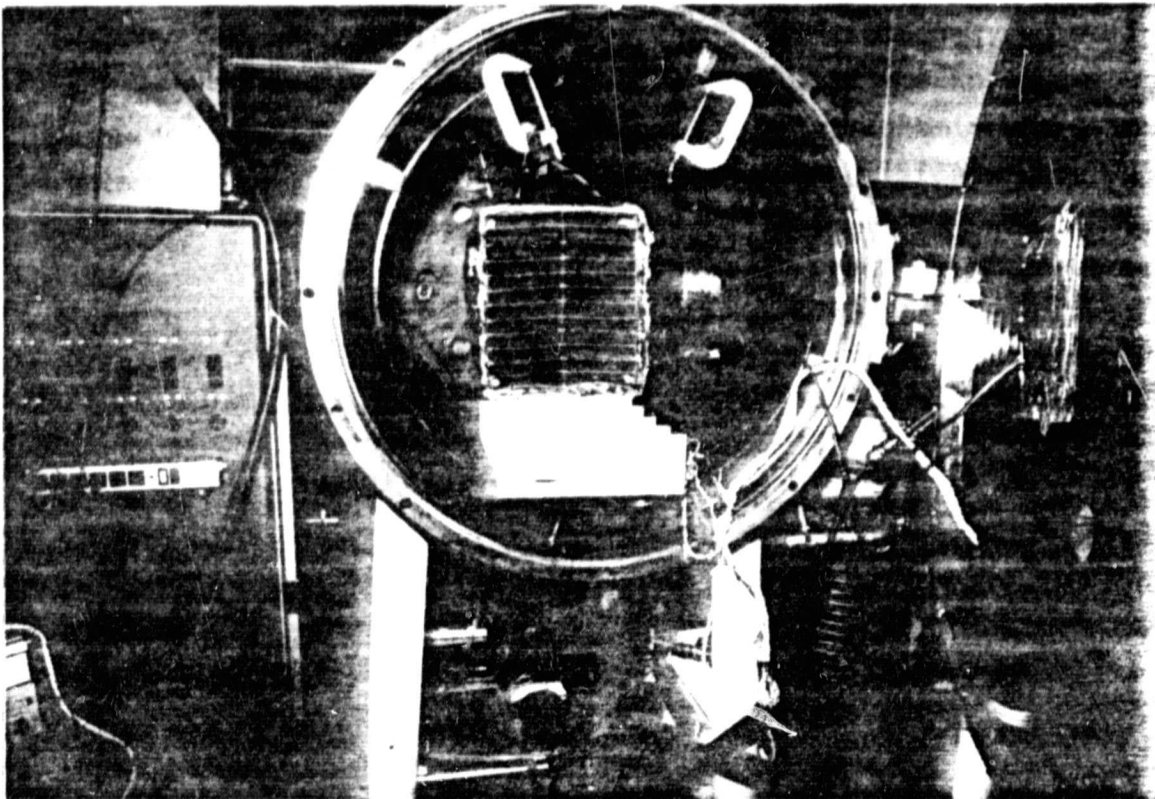


Figure 10C. Test Article Installed in Chamber.

TEST CONFIGURATION AND INSTRUMENTATION

The thermal-vacuum test was accomplished in an Ilikon model 75 vacuum chamber at Acton Environmental Testing, Acton, Massachusetts. This chamber is of the form of a horizontal cylinder, with an internal cryogenically-cooled shroud 50 inches long by 26 inches diameter. With the diffusion pump, cold trap and shroud in operation a vacuum of 10^{-6} torr or better is obtainable. The test article was suspended in the center of the chamber with nylon cord with the active surfaces facing the chamber ends. Figure 10C shows the test article in the chamber before installation of the protective cover model. A Hewlett-Packard 6228B dual DC supply powered the heaters on the test plates. Voltage and heater resistance were measured at the power supply at equilibrium for each case using a Fluke digital voltmeter; power to each heater was calculated after a correction for lead resistance. Temperatures were recorded continuously during each test with a Honeywell 24-point strip chart recorder. The test sequence is outlined in Table 1.

Table 1. LAMAR Precollimator Thermal-Vacuum Test Sequence

Day One

Side 1: 24-cell precollimator with protective cover

Side 2: 4-cell (cruciform) precollimator

Day Two

Side 1: 24-cell precollimator with no protective cover

Side 2: Open precollimator (perimeter only) with
cruciform section removed

Day Three

Side 1: 12-cell precollimator, no protective cover

Side 2: Open precollimator with protective cover

MODELING OF TEST CONFIGURATION, PREDICTIONS

The principal purpose of the precollimator tests was to verify the analytical thermal models used for prediction. It was therefore necessary to revise the original analytical models to conform as closely as possible to the actual test configuration including actual dimensions vignetting of the simulated aperture by the finite thickness of the precollimator elements, and losses through perimeter superinsulation blankets.

The honeycomb-surface heater plate was modeled using an emittance of 0.99. Test plate temperature was taken as the actual value measured for each case. Precollimator elements were modeled in four levels and the protective cover, where applicable, in two levels. Surface emittance was modeled as 0.9, a typical value for plastic several mils thick (for an intermediate diffuse surface in radiative equilibrium the surface emittance has only a second order effect). Conductance of the elements was calculated for an equivalent thickness of epoxy plastic based on a measured mass per unit area; this approximation is adequate because conduction effects were shown to be very small in any case.

The perimeter insulation blankets represent a source of uncertainty in predicted power levels. Effective emittances of 0.02 and zero (adiabatic) were assumed to bracket the possible blanket effects; the difference between these two values cause 0.4 watt difference in power prediction. This is included as one component of the range given for each power prediction.

A second component of uncertainty is the measurement of test plate temperature. Test data typically indicated a spread of as much as 4°C among three or four sensors on the plate, although 1-2°C was more typical. The spread probably was caused by slight differences in location of the thermocouple junctions from the plate surface to the top of the honeycomb. Averages were calculated to represent plate temperatures, but the actual effective radiative source temperature may have been different by the order of 1°C. The error associated with a 1°C uncertainty is proportional to the difference of T^4 , or about 1.4%, which corresponds to an error in power estimates of 0.14 watt for 10 watts total power and 0.35 watts for 25 watts of power. The same order of error may be present in the accuracy of sensors and temperature

recorder in measurement of absolute temperature, which may be 1-2°C. An uncertainty range of $\pm 3\%$ was assigned to the sum of these two effects, and is included in the range of power predictions. Table 2 compares calculated power from each test with the predictions from the analytical model. Four cases agree closely with the normal predictions before uncertainties are added; in two cases the test data are beyond the uncertainty range by 0.3 watts, or within 2%. This is considered to be excellent agreement, especially considering the large temperature differences that exist in such a configuration.

Table 2. Comparison of Test Results and Predictions

| CASE | Test Conditions | | Predicted Power | |
|-----------------|-------------------|-------------------------------|--------------------|------------------------|
| | Temperature °C | Power ¹ (watts) | Nominal (watts) | Error Range (watts) |
| 24-cell + cover | 13 | 9.4 | 9.2 | 9.1-10.1 |
| Cruciform | 14 | 18.9 | 18.7 | 18.2-19.6 |
| 24-cell | 14 | 10.4 | 10.0 | 10.1-11.1 |
| Open | 13 | 24.3 | 22.3 | 22.2-24.0 |
| 12-cell | 16 | 15.4 | 13.3 | 13.9-15.1 |
| Open + cover | 11 | 20.2 | 19.4 | 18.9-20.3 |

¹ Corrected for lead resistance

Note: Predicted power differs from corresponding values in Figure 7 because the test prediction model uses:

- actual test temperatures instead of 20°C
- actual test article area instead of 900cm²
- finite thickness of precollimator slats instead of zero.

CONCLUSIONS

Two major conclusions may be drawn from the results of the precollimator test.

- o The precollimator is effective in reducing heat flow from a telescope aperture, radiating as a blackbody;
- o Performance of a precollimator can be predicted with sufficient accuracy by conventional analytical modeling methods.

The precise performance required for LAMAR precollimator will depend on the exact configuration to be used, especially in electronics power and number of telescopes. The range of values included in this test was sufficient to bracket the likely performance requirements, and a detailed design may, therefore, be done with confidence that the desired performance can be obtained.